Pathogen-driven induction of a host transcriptome facilitating epithelial-to-mesenchymal transition

Running Title: Pathogen-driven pro-EMT induction

Liam T. Caven[1,2], Amanda J. Brinkworth[1], and Rey A. Carabeo[1,*]

[1]Department of Pathology and Microbiology, University of Nebraska Medical Center, Omaha, NE, USA.
[2]School of Molecular Biosciences, College of Veterinary Medicine, Washington State University, Pullman, WA, USA

* Rey A. Carabeo

Email: rey.carabeo@unmc.edu

Author Contributions: Conceptualization, L.C. and R.C.; Methodology, L.C., A.B., and R.C.; Validation, L.C. and A.B.; Formal Analysis, L.C.; Investigation, L.C. and A.B.; Resources, R.C.; Data Curation, L.C.; Writing – Original Draft, L.C.; Writing – Review & Editing, R.C. and A.B.; Visualization, L.C.; Supervision, R.C.; Project Administration, R.C.; Funding Acquisition, R.C.

Competing Interest Statement: The authors declare no competing interests.

Classification: Microbiology, Cell Biology

Keywords: *Chlamydia trachomatis*, YAP, fibrosis, epithelial-to-mesenchymal transition, myosin II, Hippo kinase

Summary Statement: We present a means by which *Chlamydia trachomatis* induces pro-EMT gene expression in the host via Hippo-independent, chlamydial effector-mediated activation of the transcription factor YAP.

Abstract

Chronic infection of the female reproductive tract by *Chlamydia trachomatis* can cause fibrotic infertility. Thought to be the product of the immune response to infection, the incidence of fibrosis observed in subclinical or asymptomatic infections remains unexplained. Recent work demonstrates infection induces the pro-fibrotic process of epithelial-to-mesenchymal transition (EMT), but the mechanisms underlying this are unclear. We show the *Chlamydia*-induced host transcriptome includes targets of YAP, a pro-EMT transcriptional coactivator. We observe increased YAP nuclear translocation and pro-EMT YAP target gene induction during infection, bypassing YAP inhibition by the Hippo kinase cascade, and acting via YAP tyrosine phosphoactivation associated with host Src activity, and the myosin-modulating chlamydial effector CTL0480. Comparing the host transcriptome of a ΔCTL0480-mutant infection to wild-type infection revealed consistent reduction in known YAP target expression, as well as attenuated induction of EMT. Our results define a mechanism for *Chlamydia*-directed modulation of host gene expression, providing insight into chlamydial induction of immune-independent fibrosis.

Significance Statement

Our study presents a means by which *C. trachomatis* induces pro-EMT gene expression in host epithelial cells, providing an explanation for how subclinical or asymptomatic chlamydial infections frequently result in severe fibrotic sequelae. We identify chlamydial induction of YAP activity as a principal mediator of this

effect, and thus a potential therapeutic target for *Chlamydia*-induced fibrosis. Our finding that the chlamydial effector CTL0480 – previously reported to regulate activity of non-muscle myosin II - promotes YAP activity corroborates recent discoveries indicating YAP's mechanoresponsive function can circumvent its canonical inhibition by the Hippo kinase cascade. Collectively, our data illustrates an underappreciated aspect of the host-pathogen interaction: the downstream consequences of pathogen effector activity on host gene expression.

Main Text

Introduction

Chlamydia trachomatis is the most common bacterial cause of both sexually transmitted disease and infectious blindness worldwide. Chronic or repeated *C. trachomatis* infection is associated with severe fibrotic sequelae. Ocular infection by *C. trachomatis* serovars A-C of the conjunctiva, excess collagen deposition and contraction result in the inward turning of the upper eyelid and subsequent corneal abrasion by the eyelashes (Lansingh, 2016; Taylor et al., 2014). Similarly, chronic infection of the female genital tract by *C. trachomatis* serovars D-K has been associated with pelvic inflammatory disease (PID), as well as progressive scarring of the fallopian tubes (Brunham et al., 1988; Haggerty et al., 2010; Ness et al., 2008; Robertson et al., 1987, 198; Weström et al., 1992). Blockage of the upper genital tract prevents descent of the ovum, resulting in tubal factor infertility (TFI) or ectopic pregnancy (Chow et al., 1990). In the United Kingdom, *C. trachomatis* is estimated to account for 29% of all cases of TFI, which in turn represents 25% of all cases of female infertility (Price et al., 2016). This urgent concern to public health has made understanding the pathogenesis of *C. trachomatis*-associated scarring a subject of ongoing investigation.

Initial study of the host response to infection has made a persuasive argument for chlamydial fibrosis being the product of cytokine signaling involving three key cellular players – epithelial cells, immune cells, and fibroblasts. Clinical infections have revealed substantial infiltration of infected tissues by immune cells *in vivo*, suggesting that infected epithelial cells recruit components of the innate and adaptive immune systems to the site of infection (Kiviat et al., 1990; Stephens, 2003). Indeed, upregulation of an expansive portfolio of inflammatory cytokines has been consistently observed in chlamydial infections *in vitro*, including GROα, GM-CSF, IL-1α, IL-6, IL-11, and IL-8 (Cheng et al., 2008; Eckmann et al., 1993; Rasmussen et al., 1997). IL-6 and IL-11 are particularly of note, given that both cytokines have been implicated in hepatic and pulmonary fibrosis (Epstein Shochet et al., 2020; Ng et al., 2019, 11; Ng et al., 2020, 11; Papiris et al., 2018; Widjaja et al., 2019; Xiang et al., 2018). *C. trachomatis* has also been shown to induce upregulation of signaling factors associated with fibroblast activation and wound healing such as EGF and TGF-α/β (Fischer, 2002; Igietseme et al.; Patel et al., 2014). The related species *C. pneumoniae* exhibits similar induction of pro-inflammatory and pro-fibrotic signaling, indicating this aspect of pathogenesis may be conserved amongst *Chlamydiae* (Carratelli et al., 2007; Paolillo et al., 2012). Taken together, these observations reinforce the cellular paradigm of pathogenesis put forward by Stephens in 2003: infected epithelial cells recruit an inflammatory response associated with immune cell infiltration and tissue remodeling, which during persistent or repeated infection can lead to dysregulated fibroblast activation and scarring.

While the pro-inflammatory host response to infection explains the tissue damage often associated with acute and chronic chlamydial infections, it does not account for the fibrotic outcomes of asymptomatic infection. Given estimates that up to 75% of *C. trachomatis* infections go unreported due to absent or subclinical symptoms – and that up to 18% of such cases are believed to cause infertility – it is necessary to understand how infections with an attenuated or absent inflammatory response to the

pathogen result in scarring pathology (Haggerty et al., 2010). Mounting evidence suggests that epithelial cells infected with *C. trachomatis* are altered to induce fibrosis.

Supporting this hypothesis is the recent finding that *Chlamydia* induces the epithelial-to-mesenchymal transition (EMT) in host epithelial cells, including upregulation of mesenchymal markers such as N-cadherin, MMP9, and fibronectin, as well as the pro-EMT regulators ZEB1/2, Snail1/2, and thrombospondin 1 (Igietseme et al., 2015; Igietseme et al., 2018; Rajić et al., 2017). Epithelial cells undergoing EMT transdifferentiate into a fibroblast-like phenotype, subsequently remodeling the extracellular matrix (ECM) to facilitate activation of stromal fibroblasts, collagen deposition, and scar formation (Lamouille et al., 2014; Wynn, 2008; Xu et al., 2009). Indeed, EMT has been repeatedly implicated in the progression of idiopathic pulmonary fibrosis and other scarring-associated diseases (Kyung et al., 2018; Phan et al., 2021; Salton et al., 2019). The additional finding that *Chlamydia*-infected cells produce fibroblast-activating cytokines, ECM components (collagens, laminins), and ECM-modifying matrix metalloproteases lends credence to a model of chlamydial fibrosis enhanced by, but not necessarily dependent upon, an inflammatory response to infection (Humphrys et al., 2013; Porcella et al., 2015).

The mechanism of *Chlamydia*-induced fibrosis is not completely understood. While the observed chlamydial EMT phenotype has been associated with the differential expression of specific microRNAs (Igietseme et al., 2015), the effect of infection on known pro-EMT transcription factors and other, complementary mechanisms of pro-fibrotic gene expression has been largely unexplored. Thus, we have employed *C. trachomatis* infection of End1 E6/E7-immortalized endocervical epithelial cells to perform unbiased discovery of *Chlamydia*-induced pro-EMT transcription factors (Fichorova et al., 1997). In this report, we show that *C. trachomatis* infection activates YAP, an EMT-mediating transcriptional coactivator (Noguchi et al., 2018; Panciera et al., 2017; Piersma et al., 2015), and confirmed this effect in primary endocervical epithelial cells. We subsequently demonstrate that infection promotes YAP activity via its enhanced nuclear translocation. YAP activation did not involve any apparent modulation by *Chlamydia* of Hippo kinase cascade-dependent inhibition, but instead correlated with an increase in YAP phosphorylation at Y357, a modification recently shown to enhance YAP activation (Smoot et al., 2018; Sugihara et al., 2018). Further, the activity of host kinases FAK and Src, and the chlamydial effector CTL0480, a modulator of non-muscle myosin II contractility and cytoskeletal tension (Lutter et al., 2013), are necessary for nuclear translocation. Indeed, epithelial cells infected with the ∆CTL0480 mutant produced a transcriptome exhibiting a downregulated YAP/EMT regulon relative to cells infected with wild-type *Chlamydia*. With these data, we define the initial framework by which *C. trachomatis* trigger epithelial cells to facilitate fibrosis in a manner that bypasses immune cell-mediated inflammation.

Results

Chlamydia infection induces a pro-fibrotic transcriptomic response consistent with YAP activation.

To identify host pro-EMT transcription factors induced by *Chlamydia* infection, we opted to use immortalized, non-transformed endocervical epithelial cells (End1/E6E7) as a model for infection of the upper female genital tract. We first confirmed the non-tumorigenic growth properties of End1 cells via organotypic culture on collagen rafts. Transformed cervical epithelial cells form irregular layers when induced to differentiate by exposure to the air-liquid interface (Aasen et al., 2003). By contrast End1s grown via RAFT culture formed epithelial tissues of uniform thickness (Supplemental Figure S1), consistent with previous reports of organotypic culture with this cell line (Gali et al., 2010). Having thus validated our experimental model, we then infected End1s with the genetically tractable lymphogranuloma venereum serovar L2, then harvested RNA for bulk RNA-sequencing at 24 hours post-infection (hpi).

Infection induced the differential expression (FDRP ≤ 0.05) of 3611 genes relative to a mock-infected control (Figure 1A, Supplemental Dataset S1, GEO Accession: GSE180784).

We then inferred chlamydial modulation of host transcription factors by cross-referencing this differentially expressed gene set with the ChIP Enrichment Analysis (ChEA) database of transcription factor gene targets (Lachmann et al., 2010). Of the 199 transcription factors included in ChEA, 149 exhibited twice as many induced target genes (FC ≥ 1.5) as repressed target genes (FC ≤ 1.5), suggesting chlamydial induction of transcription factor activity (Supplemental Dataset S2). Critically, targets of transcription factors known to regulate the inflammatory response to infection (IRF1, STAT1, STAT3) and pro-fibrotic gene expression (SMAD2/3, EGR1, TEAD4, YAP1) appeared to be highly induced in the host, in contrast to other pro-EMT transcription factors (e.g., MYCN and MYBL2) and unrelated regulators of gene expression (such as the photoreceptor homeobox protein CRX) (Table 1). Of note is the observed induction of gene targets of YAP1, a transcriptional coactivator known to enhance SMAD2/3, EGR1, and TEAD-family transcription factor activity, as well as induce EMT (Grannas et al., 2015; Szeto et al., 2016; Yamaguchi and Taouk, 2020; Zagurovskaya et al., 2009; Zanconato et al., 2015; Zhao et al., 2008). While YAP1 target gene induction was modest compared to other pro-EMT transcription factors identified by this analysis, modulation of YAP activity by infection (and, by extension, activity of YAP binding partners) nevertheless suggests a means by which *Chlamydia* induces pro-fibrotic gene expression in the host. Subsequent cross-reference of the differentially expressed gene set with the Comparative Toxicogenomics Database of known fibrotic genes indicated that many YAP targets induced by *Chlamydia* infection have been implicated in fibrotic pathology (Figure 1B, Table 2) (Davis et al., 2021; Davis et al.; Mattingly et al., 2006). To confirm that the observed induction of YAP-associated gene expression is also exhibited by non-immortalized cells, we then sequenced total RNA from primary human endocervical epithelial cells (HCECs) infected with *Ct* serovar L2 (Supplemental Dataset S3, Accession: GSE180784). Expression of both pro-fibrotic (CTD) and YAP-responsive (ChEA) genes by infected End1s and HCECs exhibited significant correlation (Figure 1C-1E), indicating the activation of a conserved, putatively fibrotic transcriptional program. Taken together, these data imply that chlamydial infection may modulate host gene expression via induction of YAP activity.

Chlamydia infection induces host YAP nuclear translocation and YAP/TEAD-dependent gene expression.

The mechanisms regulating YAP have been extensively studied; consistently, the transcriptional coactivator's ability to access the nuclear compartment and its DNA-binding partners correlate with YAP-mediated gene expression (Dasgupta and McCollum, 2019; Pocaterra et al., 2020). Thus, we opted to confirm the hypothesis that chlamydial infection promotes YAP activity by assaying the nuclear incidence of YAP in serovar L2-infected cells via immunofluorescence. Consistent with our initial observation of YAP target gene induction, nuclear YAP was increased in *Chlamydia*-infected End1/E6E7 cells at 24 hpi, relative to mock-infected control cells (Figure 2A). To account for variations in nuclear size and staining efficiency, we subsequently performed blind quantification of randomly selected nuclei in each sample, measuring ratios of nuclear to cytosolic YAP. Consistently, infection was concomitant with a statistically significant, 1.5-fold increase in nuclear-to-cytosolic YAP ratio relative to mock-infected cells (Figure 2B). Given that expression of HPV proteins E6 has been shown to stabilize YAP and thereby modulate its activity (He et al., 2015; Strickland et al., 2018), we assayed nuclear YAP translocation in HCECs as well, observing an equivalent increase to that in E6-expressing End1s (Figure 2C, 2D). Collectively, these data indicate chlamydial induction of YAP irrespective of HPV E6/E7 expression.

To confirm that *Chlamydia*-induced pro-fibrotic gene expression was driven by YAP activity, we examined expression of YAP target genes in the presence of verteporfin, an inhibitor of YAP-TEAD complex formation (Szeto et al., 2016; Wei et al., 2017). Consistent with our previous data, analysis of host gene expression via RT-qPCR demonstrated the induction of known YAP-responsive, pro-EMT genes, including inhibin beta A (INHBA) and bone morphogenetic protein 2 (BMP2) (Bashir et al., 2015; Herrera et al., 2017; Huang et al., 2016; Huang et al., 2017; Mo et al., 2012). Expression of connective

tissue growth factor (CTGF) – a consistent marker of YAP target gene induction – was similarly increased in response to infection (Futakuchi et al., 2018; Zhao et al., 2008) (Figure 2E). Increased expression of all three YAP-responsive genes was significantly attenuated by 2 to 2.5-fold by verteporfin treatment, implying that pro-fibrotic gene expression during infection is dependent upon YAP-TEAD complex formation. Intriguingly, while infection significantly induced expression of the pro-EMT transcription factor SNAIL, SNAIL expression was not similarly inhibited by verteporfin, suggesting a component of chlamydial EMT induction is likely independent of YAP-TEAD complex formation. Collectively, these results show that *Chlamydia*-infected cells exhibit increased YAP activation, resulting in pro-EMT gene expression.

***Chlamydia* infection activates host YAP by circumventing Hippo-mediated YAP inhibition.**

In confluent epithelial cells, YAP's access to the nuclear compartment is inhibited by the Hippo kinase complex stabilized by cell-cell contact. The resulting phosphorylation cascade inhibits YAP via phosphorylation at specific serine residues (Piccolo et al., 2014). Recent work has also shown that YAP nuclear translocation is enhanced by signaling at focal adhesions and stress fibers, constituting a response to mechanical stimuli such as cell spreading, substrate stiffness, and tension across the actin cytoskeleton (Dasgupta and McCollum, 2019; Driscoll et al., 2015; Sero and Bakal, 2017; Vite et al., 2018, 201). To determine which structures are modulated by *Chlamydia* to induce YAP activity, we examined YAP activation in culture conditions of inhibited cell-cell contact. By seeding End1/E6E7 cells on glass treated with fibronectin in 30- and 45-μm micropatterns, the resulting deposition of small cell clusters allowed us to assay YAP nuclear translocation in an environment where adherens junctions and other cell-cell contacts were absent or severely limited. In both 30-μm patterns (1-3 cells/cluster) and 45-μm patterns (2-4 cells/cluster), we observed a significant increase in YAP nuclear translocation in serovar L2-infected cells at 24 hpi, relative to mock-infected controls (Figure 3A). Consistent with our previous observations in confluent End1/E6E7 monolayers, quantification of our immunofluorescence data indicated that infection promotes a 1.5-fold increase in YAP activation relative to uninfected cells in this sub-confluent culturing condition (Figure 3B). This phenotype was additionally observed when adherens junction was disassembled by calcium chloride withdrawal in confluent *Chlamydia*-infected End1/E6E7 monolayers (Supplemental Figure S2) (Brown and Davis, 2002; O'Keefe et al., 1987). Taken together, these data suggest that chlamydial activation of YAP occurs independently of signaling at adherens junctions – and by extension, YAP inhibition by the Hippo kinase cascade.

The recruitment of Hippo cascade members to adherens junctions promotes the formation of a YAP-inhibitory complex, resulting in YAP phosphorylation at serine residues by Hippo complex members LATS1/2 (Dong et al., 2007; Lei et al., 2008; Zhao et al., 2007b). By contrast, YAP activation by stress fibers and focal adhesions is associated with Hippo-independent phosphorylation of YAP at Y357 and other tyrosine residues, facilitating YAP's nuclear retention (Elbediwy et al., 2016; Elbediwy et al., 2018). To confirm that chlamydial YAP activation occurred via Hippo-independent signaling, we thus examined YAP phosphorylation in cells growing at full confluency and infected with *Chlamydia* via Western blotting. Serovar L2-infected End1/E6E7 cells exhibited increased YAP Y357 phosphorylation at 24 hpi relative to a mock-infected control, consistent with mock-infected cells treated with sodium orthovanadate (Na_3VO_4), a tyrosine phosphatase inhibitor that has been previously used as a positive control for increased YAP tyrosine phosphorylation (Figure 3C, 3D) (Sugihara et al., 2018). Surprisingly, L2-infected cells did not exhibit altered YAP S127, suggesting that infection does not relieve Hippo-mediated YAP inhibition (Figure 3C, 3E). By contrast, pY357-YAP levels were increased in an infection-dependent manner. At present, it is unclear if pY357-YAP is also phosphorylated at S127, or if we are observing independent pools of phosphorylated species of YAP. Regardless, these data demonstrate that infection renders ineffective the S127 phosphoinhibition event typically associated with the Hippo kinase cascade, while promoting alternative phosphoactivation of YAP at Y357.

YAP activation at Y357 has been attributed to the activity of focal adhesion kinase (FAK) and Src-family kinases (Elbediwy et al., 2018; Lachowski et al., 2018; Smoot et al., 2018; Sugihara et al., 2018).

To determine if infection-mediated YAP activity is the product of this Hippo-independent mechanism of YAP regulation, we attenuated the YAP activation phenotype via inhibition of either FAK or Src. Consistent with our hypothesis, treatment of serovar L2-infected cells with the FAK inhibitor PF-573228 or the Src inhibitor PP2 over the course of a 24-hour infection resulted in a statistically significant attenuation of YAP nuclear translocation relative to a DMSO-treated control (Figures 3F, 3G). YAP phosphorylation at Y357 in infected cells was also severely attenuated by Src inhibition (Figure 3H), consistent with studies implicating Src-family kinases in YAP tyrosine phosphorylation (Smoot et al., 2018; Sugihara et al., 2018). Intriguingly, FAK inhibition did not reduce Y357-pYAP relative to the vehicle-treated infection – a surprising result, given this treatment attenuated nuclear incidence of YAP in infected cells. This discrepancy could be due to an alternative means of regulating YAP nuclear translocation. Indeed, FAK knockout can enhance inhibitory serine phosphorylation of YAP at S397, consistent with the observed decrease in nuclear YAP despite no reduction in the level of pY357-YAP (Hu et al., 2017). Taken together, these data indicate that chlamydial induction of YAP activity occurs independent of cell-cell contact and inhibition by the Hippo kinase cascade, and instead likely enhanced by Src- mediated responses to cell-substrate contact and cytoskeletal tension.

Chlamydial YAP activation requires the myosin-modulating effector CTL0480.

To confirm that the observed increase in YAP activity was a *Chlamydia*-driven process requiring the action of one or more chlamydial effectors, we next examined YAP activation via immunofluorescence over the course of a 24-hour infection, as to identify a stage at which inhibition of chlamydial effector synthesis would be most effective. While we observed a significant increase in YAP activation between mock- and serovar L2-infected End1/E6E7 cells as early as 8 hpi, a statistically significant increase between infected cells was first detected between 12 and 18 hpi, indicating that synthesis of YAP-modulating chlamydial effectors may occur at this stage of infection (Figure 4A). We next attempted to attenuate chlamydial YAP induction at 18 hpi via treatment with chloramphenicol, an inhibitor of bacterial protein synthesis. In agreement with our initial hypothesis, chloramphenicol treatment for one hour prior to fixation at 18 hpi was sufficient to significantly inhibit YAP nuclear translocation relative to a DMSO-treated control (Figures 4B, 4C). Given these data, we conclude that YAP activation in infected cells required *de novo* synthesis of chlamydial effectors.

Importantly, specific chlamydial effectors have been reported to modulate host cell focal adhesion stability and cytoskeletal tension, and may thereby promote YAP activation. The highly conserved secreted chlamydial effector TarP was recently shown by our laboratory to have a post-invasion role in enhancing focal adhesion stability through reduction in turnover rates (Pedrosa et al., 2020). Additionally, the chlamydial protein CTL0480 has been shown to modulate myosin contractility via the sequestration of MYPT1 to the inclusion membrane (Lutter et al., 2013). MYPT1 modifies protein phosphatase 1c substrate specificity to myosin light chain-2, thereby reducing myosin II contractility (Eto et al., 2005; Grassie et al., 2011; Joo and Yamada, 2014, 1; Korrodi-Gregório et al., 2014, 1). MYPT1 sequestration away from its site of action increases tension at those structures; indeed, sequestration of MYPT1 at the chlamydial inclusion membrane promotes tension-dependent thickening stress fibers. Cells infected with a *C. trachomatis* mutant lacking CTL0480 produced markedly thinner stress fibers (Murphy and Carabeo, submitted). Critically, both focal adhesions and cytoskeletal tension have been shown to regulate YAP in Hippo-independent fashion (Dasgupta and McCollum, 2019); thus, we next evaluated the capacity of CTL0480 and TarP to activate YAP. Confluent End1/E6E7 cells were infected with TarP- or CTL0480-deficient serovar L2 mutant strains (Ghosh et al., 2020; Lutter et al., 2013), then assayed for YAP nuclear translocation relative to a wild-type infected control. While L2ΔCTL0480-infected cells were YAP-attenuated relative to wild-type infection at 24 hpi (Figures 4F, 4G), L2ΔTarP-infected cells were not (Figures 4D, 4E). Consistent with this finding, we observed a similar YAP-attenuated phenotype in cells infected with the ocular serovar B (Supplemental Figure S3A, S3B), which possesses a pseudogene predicted to encode a nonfunctional CTL0480 homolog due to premature translation termination (Lutter et al., 2013). Additionally, YAP Y357 phosphorylation in the CTL0480 mutant and serovar B infections was

not significantly different from either mock or L2 wild-type controls (Supplemental Figure S3C, S3D), suggesting loss of CTL0480 partially attenuates Src-dependent YAP phosphoactivation to produce an intermediate phenotype. Taken together, these results indicate that YAP induction in *Chlamydia*-infected epithelial cells is a pathogen-driven process requiring the inclusion membrane protein CTL0480, a likely contributor to Src-mediated YAP phosphoactivation.

Loss of CTL0480 attenuates *Chlamydia*-induced pro-fibrotic gene expression.

Given the observed attenuation of YAP nuclear translocation in the L2ΔCTL0480 infection and the potential for the CTL0480's myosin-regulating activity to modulate other mechanoresponsive transcription factors, we next opted to determine the specific effect of CTL0480 on the host transcriptome during infection. To this end, we isolated RNA from End1 cells infected either with *Ct* serovar L2 wild-type or L2ΔCTL0480, then assayed their relative host gene expression via bulk RNA-sequencing. Relative to the wild-type control infection, the ΔCTL0480 strain induced the differential expression of 315 host genes (FDRP <= 0.05), of which nearly half (158) were present within the CTD set of known fibrotic genes (Figure 5A, 5B, Supplemental Dataset S3, GEO Accession: GSE180784) (Davis et al., 2021; Mattingly et al., 2006). Intriguingly, only 35 pro-fibrotic genes also mapped to the ChEA target list for YAP (Lachmann et al., 2010). The majority of differentially expressed YAP targets were modestly downregulated relative to the wild-type infection – consistent with the intermediate YAP activation phenotype observed in a CTL0480-deficient infection (Supplemental Dataset S4). However, the fact that known YAP target genes constitute only a minority of the differential pro-fibrotic gene expression observed here strongly implies that CTL0480 may modulate additional transcription factors.

Within the CTL0480-deficient infection transcriptome, the top 25 significantly enriched ($p \leq 0.05$) GO terms included extracellular matrix reorganization, TGF-β production and signaling, and positive regulation of EMT (Figure 5C). Critically, genes annotated with these terms appear consistently downregulated (Supplemental Figure S4), suggesting a principal effect of CTL0480 on the host transcriptome is to enhance pro-fibrotic gene expression. Subsequent confirmation of expression levels via qRT-PCR showed the induction of INHBA previously observed in wild-type infection is significantly attenuated in a CTL0480-deficient background (Figure 5D). Loss of CTL0480 also attenuated expression of additional YAP-responsive genes as identified by the ChIP Enrichment Analysis database (Lachmann et al., 2010): PELI1, an E3 ubiquitin ligase that stabilizes SNAIL to facilitate EMT induction (Jeon et al., 2017), and ESM1, a soluble proteoglycan implicated in renal EMT activation (Hung et al., 2020). Taken together, these data indicate loss of CTL0480 results in attenuated pro-EMT gene induction in the host and reduced expression of YAP target genes, in accordance with our hypothesis that CTL0480 enhances YAP-mediated pro-EMT gene expression.

Only a minority of host genes downregulated in a CTL0480-deficient infection are known targets of YAP, emphasizing the potential for CTL0480 to modulate other host transcription factors. Supporting this is the observation of CTL0480-dependent expression of known SNAIL modulator PELI1, despite chlamydial induction of SNAIL exhibiting insensitivity to YAP inhibition by verteporfin. Given the reported function of CTL0480 as a regulator of myosin light chain-2 activity and cytoskeletal tension (Lutter et al., 2013), the possibility that this effector modulates other mechanoresponsive transcription factors is difficult to ignore. One attractive target for further investigation is the myocardin-related transcription factor (MRTF) family, comprising myocardin, MRTF-A, and MRTF-B (Finch-Edmondson and Sudol, 2016). Importantly, MRTF-A is sequestered in the cytoplasm when bound to monomeric actin, translocating to the nucleus to promote gene expression in response to changes in actin polymerization (Miralles et al., 2003). Serum response factor (SRF) has also been implicated in mechanotransduction: the application of tension to cardiac fibroblasts is shown to induce expression of the SRF target α-smooth muscle actin (Zhao et al., 2007a). Given that EMT has been associated with dysregulation of both SRF and MRTF (Gasparics and Sebe, 2018; Korol et al., 2016; Morita et al., 2007), investigation of CTL0480's capacity to modulate these transcription factors – as well as the specific effect of its activity on host cytoskeleton dynamics – appears warranted.

Discussion

In this report, we present a novel mechanism for pro-EMT gene expression in *Chlamydia*-infected epithelial cells. Infection of epithelial cells with *C. trachomatis* serovar L2 resulted in robust expression of pro-fibrotic genes in a manner consistent with induction of the pro-EMT transcriptional coactivator YAP and its DNA-binding partners. Consistent with this observation, infected cells also exhibit increased YAP nuclear translocation. This phenotype was concomitant with increased SNAIL expression, as well as expression of YAP target genes CTGF, INHBA, and BMP2 (an effect sensitive to inhibition of YAP-TEAD complex formation). Chlamydial modulation of YAP appears to bypass the latter's inhibition by the Hippo kinase cascade, given that Hippo-mediated phosphorylation of YAP at S127 was unchanged by infection, and increased YAP activation was observable in sub-confluent cells. Instead, infection acts upon an alternative, Hippo-independent pathway involving phosphorylation of YAP at Y357 and the activity of host kinases FAK and Src. Finally, we show that the chlamydial inclusion protein CTL0480 promotes YAP activation, and that loss of CTL0480 results in reduced YAP nuclear translocation, attenuated host expression of pro-EMT genes such as ESM1, INHBA, and PELI1, and an overall transcriptome with decreased representation of pro-EMT and pro-fibrotic genes.

Our assessment of CTL0480 as a YAP-activating bacterial effector is consistent with data indicating that YAP is modulated by other bacterial pathogens. The Gram-negative pathogen *Helicobacter pylori* was recently shown to enhance YAP expression through the action of the effector CagA (Li et al., 2018). It is unclear how CagA interacts with the steady-state inhibition of YAP by the Hippo kinase cascade; given the prior finding that CagA destabilizes host cell-cell junctions – a common site of Hippo kinase complex recruitment – one possible explanation is that CagA antagonizes Hippo-mediated YAP inhibition by indirectly preventing stabilization of the Hippo complex (Song et al., 2013). Alternatively, the observation that YAP expression is increased by CagA in a dose-dependent fashion suggests that *H. pylori* infection may instead circumvent Hippo inhibition by overwhelming either Hippo's capacity to phospho-inhibit YAP or 14-3-3's capacity to sequester serine-phosphorylated YAP in the cytoplasm (Li et al., 2018). Regardless, the observation that *H. pylori* enhances EMT in gastric epithelia in a CagA-dependent fashion is consistent with our finding of another bacterial pathogen that modulates YAP activity. The loss of chlamydial CTL0480 appears to inhibit EMT and pro-fibrotic gene expression induced by infection (Li et al., 2018; Song et al., 2013). Taken together, these results illustrate that a subset of differentially expressed host genes during infection is due to specific modulation of host transcription factors by pathogen effectors, rather than a general host response to the pathogen.

The observation that YAP nuclear translocation in the CTL0480-deficient mutant infection was still significantly increased relative to mock-infected controls suggests that other YAP-activating chlamydial effectors may supplement CTL0480 activity. One possible candidate for this effect is the chlamydial inclusion protein IncG, which has been previously shown to interact with host 14-3-3β (Scidmore and Hackstadt, 2001). Given that 14-3-3-family proteins are known to act downstream of Hippo-mediated YAP inhibition by binding and sequestering serine-phosphorylated YAP in the cytosol (Basu et al., 2003; Dong et al., 2007; Zhao et al., 2007b), potential inhibition of 14-3-3 by IncG may complement CTL0480-dependent YAP activation in decoupling YAP from Hippo-mediated phosphoinhibition. Additional YAP-activating factors may operate via enhancement of YAP tyrosine phosphorylation, an event observed concomitant with increased YAP nuclear translocation. Further, loss of CTL0480 did not completely ablate increased phosphorylation of YAP at this residue, indicating that other chlamydial effectors may act on YAP in this fashion. Given that chlamydial YAP phosphoactivation is demonstrably sensitive to inhibition of Src-family kinases, screening for chlamydial modulators of Src or signaling pathways that lead to increased Src kinase activity may identify additional YAP-activating effectors. Critically, Src family kinases have been implicated in several chlamydial processes, including phosphorylation of TarP during invasion and localization of the chlamydial inclusion to the microtubule organizing center (Jewett et al., 2008; Mital and Hackstadt, 2011). Additionally, given we observe that only one hour of inhibition of bacterial protein synthesis was sufficient to attenuate YAP activation in infected cells, CTL0480 and other YAP-activating effectors may have relatively high rates of turnover requiring regular replenishment.

Our finding that TarP is dispensable for YAP activation is surprising, given our recent report on this effector's role in promoting focal adhesion stability by inserting itself within these structures and disrupting their nanoscale organization, rather than manipulating tension (Pedrosa et al., 2020). By contrast, CTL0480 by negatively regulating MYPT1 induces thickening of stress fibers (Murphy and Carabeo, manuscript in preparation) exhibits a clearer connection to tension-dependent YAP activation as evidenced by increased Y357 phosphorylation.

While we observe that the Hippo kinase cascade was not targeted by Chlamydia to increase YAP activation, we cannot formally exclude a role for this negative regulator in determining the net level of active YAP. The recent report of chlamydial disruption of cell junctions in an organoid model of infection (Dolat and Valdivia, 2021) indicates that the Hippo pathway could still be targeted by Chlamydia, potentially cooperating with the CTL0480-dependent alternative YAP activation. Though beyond the scope of this initial study, further investigation of chlamydial YAP activation will likely necessitate use of three-dimensional culture models to determine which of the extensive portfolio of YAP-modulatory subcellular structures and mechanical inputs are co-opted by infection.

Our results put forward a potential mechanism for the recent report of YAP activation at an earlier stage of chlamydial infection (Shehat et al., 2021). The authors present the significant infection- and TarP-dependent induction of YAP target genes TEAD4 and XIAP at 8 hpi, contending the observed loss of YAP and target expression in a TarP-deficient infection indicates TarP may inhibit YAP degradation. However, the lack of involvement of TarP in YAP activation we observe later in infection calls into question the relevance of findings made at 8 hpi. Indeed, by 18 hpi it appears that CTL0480 activity on YAP supersedes TarP involvement entirely.

Given the emergence of data indicating chlamydial induction of EMT in infected cells, it seems likely that chlamydial YAP activation described here is one of several complementary mechanisms driving EMT progression during infection. Recent work studying modulation of the host phopshoproteome implicated MAPK-mediated activation of the transcription factor ETS1 in the chlamydial EMT phenotype (Zadora et al., 2019). Given that ETS1 has been repeatedly demonstrated as YAP-responsive (Kim et al., 2015; Meinhardt et al., 2020), investigation of cooperation between YAP- and MAPK-driven signaling in chlamydial EMT induction is likely to provide valuable insight. Recent study of YAP-knockout murine embryonic stem cells identified a role for the transcription factor in regulating DNA methylation; thus, the potential for chlamydial dysregulation of YAP to facilitate reported infection-associated changes in methylation of the epithelial marker E-cadherin is similarly difficult to ignore (Rajić et al., 2017). Indeed, YAP activity has been shown to repress E-cadherin while, enhancing expression of the mesenchymal marker vimentin and the pro-EMT transcription factor Slug (Cheng et al., 2020; Park et al., 2019). Given that the chlamydial EMT phenotype has been linked to differential incidence of EMT-modulating host miRNAs, work indicating that YAP interacts with p72 – a critical regulator of miRNA processing – suggests that chlamydial induction of YAP may have downstream effects on host miRNA that in turn facilitate EMT induction (Igietseme et al., 2015; Mori et al., 2014). However, the recent finding that YAP is in turn regulated by the microRNA miR-27a-3p implies that the functional relationship of YAP and miRNA activity in regulating EMT is likely much more complex (Zeng et al., 2016). Further study is necessary to determine how chlamydial modulation of miRNA and YAP interact; the YAP-attenuated, CTL0480-deficient mutant may prove an effective means of identifying the component of miRNA-mediated EMT induction reliant upon YAP activity.

While our results illustrate a mechanism by which chlamydial infection promotes YAP-dependent, pro-fibrotic gene expression in the host, the benefit of this interaction to the pathogen is unclear. Given the established function of CTL0480 in modulating chlamydial egress via regulation of myosin contractility (Lutter et al., 2013), the indirect effect of this chlamydial protein on YAP can be viewed as a downstream process relevant to histopathology, but not necessarily of benefit to the pathogen. The potential relevance to disease progression, i.e. formation of advanced sequelae such as scarring, warrants further investigation. Given past work demonstrating *Chlamydia*-infected cells exhibit increased expression of genes encoding pro-fibrotic cytokines and ECM components (Humphrys et al., 2013; Porcella et al., 2015), and our own observation that infection enhances expression of pro-fibrotic signaling factors BMP2,

INHBA, and CTGF, the possibility of infected cells inducing a fibrotic response in uninfected, “bystander” epithelial cells and stromal fibroblasts is likely. These data also form the basis of an immune response-independent means of activating fibroblasts. While fibroblasts are understood to play a critical part in driving the pathology of many scar-forming diseases (Kendall and Feghali-Bostwick, 2014), their role in chlamydial fibrosis has yet to be fully assessed. Understanding the yet uncharacterized effect of *Chlamydia*-infected cells on their uninfected neighbors will likely be critical to elucidating mechanisms of chlamydial fibrosis *in vivo*.

Materials and Methods

Eukaryotic Cell Culture and Chlamydial Infections

Human endocervical epithelial HPV-16 E6/E7 transformed End1s (End1 E6/E7, ATCC CRL-2615) were cultured at 37° C with 5% atmospheric CO_2 in Keratinocyte Serum-Free Medium (KSFM, Thermo Fisher Scientific) supplemented with human recombinant epidermal growth factor, bovine pituitary extract, 5 micrograms/mL gentamicin, and 0.4 mM $CaCl_2$ (unless otherwise indicated). For all experiments, End1s were cultured between passages 3 and 15. Primary human cervical epithelial cells (HCECs, ATCC PCS-0480-011, Lot 80306190) were cultured at 37° C with 5% atmospheric CO_2 in Cervical Epithelial Cell Basal Medium (CECBM, ATCC PCS-480-032) supplemented with all contents of a Cervical Epithelial Growth Kit (ATCC PCS-080-042). *Chlamydia trachomatis* serovar L2 (434/Bu) was originally obtained from Dr. Ted Hackstadt (Rocky Mountain National Laboratory, NIAID). L2ΔTarP and L2cisTarP mutant strains were provided by Dr. Ken Fields, and the L2ΔCTL0480 mutant strain was provided by Dr. Derek Fisher and Dr. Erika Lutter. Chlamydial EBs were isolated from infected, cycloheximide-treated McCoy cells at 36-40 hours post-infection (hpi) and purified by density gradient centrifugation as previously described (Caldwell et al., 1981). All cell lines used in this study are tested annually for mycoplasma contamination.

For infection of 6- and 24-well tissue culture plates (Greiner Bio-One 657160 and 662160), End1s seeded at 125% of confluence or HCECs grown to confluence (6-7 days) were washed with pre-warmed Hanks Buffered Saline Solution (HBSS) prior to inoculation with *Chlamydia*-containing KSFM or CECBM at a multiplicity of infection (MOI) of 5, except where otherwise indicated. Tissue culture plates were centrifuged at 4° C and 500 rcf (Eppendorf 5810 R tabletop centrifuge, A-4-81 rotor) for 15 minutes to synchronize infection. Inoculum was then aspirated, and cells were washed with chilled HBSS prior to the addition of pre-warmed KSFM or CECBM. Infected cultures were then returned to the tissue culture incubator until the indicated times post-infection. Where indicated, media was replaced with fresh, pre-warmed KSFM containing DMSO (Thermo Fisher Scientific D12345, 1:1000), verteporfin (Cayman Chemical Company 17334, 5 μM), sodium orthovanadate (Sigma-Aldrich 450243, 5 μM), PF-573228 (Cayman Chemical Company 14924, 5 μM), PP2 (EMD Millipore 529576, 10 μM), or chloramphenicol (Sigma-Aldrich C0378, 50 μg/mL). RAFT cultures were prepared as previously described by our laboratory (Nogueira et al., 2017), exchanging HaCaT cells for End1s where indicated, and cultured over 19 days before being fixed for 30 minutes in 4% paraformaldehyde, OCT-embedded, cryo-sectioned, and stained with hematoxylin and eosin.

Bulk RNA-Sequencing and Analysis

End1s seeded on fibronectin-coated 6-well plates (Corning 354402) and infected at an MOI of 2 as described above were harvested for RNA using TRIzol (Thermo Fisher Scientific 15596026) and the DNA-free DNA removal kit (Thermo Fisher Scientific AM1906), according to manufacturers’ protocols. Extracted RNA was subsequently enriched for polyadenylated mRNA transcripts using the NucleoTrap mRNA enrichment kit (Macherey-Nagel) according to the manufacturer’s protocol. For the comparison of Mock- and *Ct* serovar L2-infected transcriptomes, RNA samples were subsequently assayed for

fragmentation using an Agilent 5200 Fragment Analyzer; intact samples were enriched for polyadenylated transcripts via the NucleoTrap kit a second time due to the high incidence of ribosomal RNA in the fragment analysis results. cDNA library preparation was performed using the Ion Xpress Plus Fragment Library kit (Thermo Fisher Scientific 4471269), and sequencing of cDNA libraries was performed using the Ion Torrent system (Life Technologies).

For the comparison of wild-type L2- and L2ΔCTL0480-infected transcriptomes, as well as the bulk RNA-sequencing of primary cells, End1s or HCECs infected at an MOI of 2 were harvested for RNA samples via TRIzol and the DNA-free DNA removal kit as described above, and were subsequently assayed for fragmentation using an Agilent Bioanalyzer 2100. cDNA library preparation of intact samples was performed using the NuGEN Universal mRNA-Seq Library Preparation kit, and sequencing of cDNA libraries was performed using the NextSeq 550 system (Illumina). Read alignment and downstream analysis of both experiments was performed using CLC Genomics Workbench (Qiagen); each treatment group was comprised of libraries from three biological replicates, each with a minimum of 30 million reads each (unstranded single read, mean length 150 bp), genes with an FDRP ≤ 0.05 considered differentially expressed. ChEA crossreferencing was performed in Python, identifying the number of genes induced (FC ≥ 1.5, FDRP ≤ 0.05) and repressed (FC ≤ 1.5, FDRP ≤ 0.05) by infection for each transcription factor's gene targets (Lachmann et al., 2010). Pearson's correlation coefficients between End1 and HCEC expression were subsequently calculated in R, using log-transformed fold changes of all genes differentially expressed in at least one data set. Gene set enrichment analysis was also performed in R, using the Bioconductor package clusterProfiler (Yu et al., 2012).

Immunofluorescence Microscopy

End1s or HCECs seeded on glass cover slips (VWR) coated with fibronectin (Corning 354008) or fibronectin-deposited micropatterned chips (CYTOO) and infected as described above were fixed in 4% paraformaldehyde in phosphate-buffered saline (PBS) for 10 minutes at 37° C, washed in PBS, then blocked in 5% bovine serum albumin (BSA) in PBS for 1 hour at room temperature. Fixed and blocked cover slips were subsequently incubated overnight at 4° C with primary antibodies in 1% BSA-PBS: rabbit anti-YAP (CST 4912, 1:100 dilution), rabbit anti-E-Cadherin (CST 3195, 1:200 dilution). Cover slips were again washed in PBS, then incubated for 1 hour at room temperature with the following fluorophore-conjugated antibodies/dyes in 1% BSA-PBS: goat anti-rabbit Alexa-488 conjugate (Thermo Fisher Scientific A-11034, 1:1000 dilution), phalloidin Alexa-594 conjugate (Thermo Fisher Scientific A-12381, 1:120 dilution), DAPI (Sigma-Aldrich 10236276001, 1:1000 dilution). Afterward, cover slips were washed in PBS and ultrapure water, then mounted on microscope slides using Shandon Immu-Mount (ThermoFisher Scientific 9990402). At least 5 fields of each cover slip were imaged using a SP-8 Lightning Confocal Microscope (Leica) or CSU-W1 Spinning-Disk Confocal Microscope (Nikon). To account for variations in nuclear size and avoid biased selection of cells for measurement, blinded image quantification was performed by assigning image filenames randomized number codes, selecting 10 nuclei at random per field using only the DAPI channel, manually masking the nuclear area, and recording the mean YAP fluorescence intensity per nucleus. To account for variation in total YAP between cells and staining efficiency between cover slips, 5 cytosolic regions not occluded by an inclusion body and near to measured nuclei were selected per field, with the mean YAP fluorescence intensity of these regions averaged to produce a per-field measurement of mean cytosolic YAP fluorescence intensity; nuclear translocation of YAP was thereby expressed as a ratio of mean nuclear fluorescence to mean cytosolic fluorescence. Statistical analysis was performed in R, using a Kruskal-Wallis test to first verify a statistically significant (p-value < 0.05) difference between treatment groups. Subsequent pairwise comparisons were performed using a Wilcoxon rank sum test and Bonferroni's correction for multiple comparisons, with p-values less than 0.05 being considered statistically significant.

SDS-PAGE and Western Blotting

To minimize activity of the chlamydial protease CPAF, End1s seeded on 6-well plates and infected as described above were subsequently lysed in 1% SDS buffer heated to 95° C, as previously described (Johnson et al., 2015). After treatment with Pierce Universal Nuclease (Thermo Fisher Scientific, 1:1000 dilution) for 5 minutes at room temperature, lysates were combined with 4X Laemmli Sample Buffer (Bio-Rad 1610747) for loading on a 7.5% acrylamide/bis-acrylamide gel for SDS-PAGE (1.5 hours, 120V). Gels were then transferred to PVDF membranes (Bio-Rad 1620177) using a semi-dry transfer method. After blocking in 5% BSA in PBST (PBS containing 0.1% Tween-20) for 1 hour at room temperature, membranes were incubated overnight at 4° C with primary antibodies in 5% BSA-PBST: rabbit anti-YAP (CST 4912, 1:1000 dilution), rabbit anti-S127-pYAP (CST 13008, 1:1000 dilution), rabbit anti-Y357-pYAP (Abcam ab62571, 1:1000 dilution). Membranes were subsequently washed in PBST, then incubated with a goat anti-rabbit HRP-conjugated secondary antibody (Dako P0448, 1:2000 dilution in 5% BSA-PBST) for 2 hours at room temperature. After additional washing in PBST, membranes were imaged using Immobilon HRP Substrate (Millipore Sigma WBKLS0500) or an Azure Biosystems c600. Images were analyzed using the ImageJ gel analysis tool to quantify the fluorescence density of phospho-analyte bands relative to the YAP total protein loading control. Statistical analysis was performed in R, using pairwise Student's t-tests with Bonferroni's correction for multiple comparisons; p-values less than 0.05 were considered statistically significant.

Quantitative Real-Time PCR

End1s seeded on fibronectin-coated 6-well plates (Corning 354402) and infected as described above were harvested for RNA using TRIzol (Thermo Fisher Scientific 15596026) and the DNA-free DNA removal kit (Thermo Fisher Scientific AM1906), according to manufacturers' protocols. cDNA libraries were subsequently prepared using SuperScript IV Reverse Transcriptase (Thermo Fisher Scientific 11766050) according to the manufacturer's protocol. Quantitative real-time PCR was performed on a QuantStudio 3 (Thermo Fisher Scientific) using TaqMan assay kits of the following genes: CTGF (Thermo Fisher Scientific Hs01026927_g1), INHBA (Thermo Fisher Scientific Hs01081598_m1), SNAI1 (Thermo Fisher Scientific Hs00195591_m1), BMP2 (Thermo Fisher Scientific Hs00154192_m1), PELI1 (Thermo Fisher Scientific Hs00900505_m1), ESM1 (Thermo Fisher Scientific Hs00199831_m1), and HPRT (Thermo Fisher Scientific Hs02800695_m1). Statistical analysis was performed in R, using pairwise Student's t-tests and Bonferroni's correction for multiple comparisons; p-values less than 0.05 were considered statistically significant.

Acknowledgments

The authors acknowledge the members of the Carabeo laboratory for their critical feedback on the development of this project. We also acknowledge the generosity of Drs. Ken Fields, Derek Fisher, and Erika Lutter who provided the mutant chlamydial strains used in this study, as well as the WSU SMB Genomics Core and UNMC Genomics Core for performing mRNA library preparation and bulk RNA-sequencing, and the UNMC Tissue Science Facility for RAFT culture sectioning and slide preparation.

Competing Interests

The authors declare no competing interests.

Funding

This work was supported by NIAID grant R01 AI065545 to RAC. The University of Nebraska DNA Sequencing Core receives partial support from the National Institute for General Medical Science (NIGMS) INBRE - P20GM103427-19 grant as well as The Fred & Pamela Buffett Cancer Center Support Grant - P30 CA036727. This publication's contents are the sole responsibility of the authors, and do not necessarily represent the official views of the NIH.

Data Availability

The bulk RNA-sequencing data discussed in this publication have been deposited in NCBI's Gene Expression Omnibus (Edgar et al., 2002) and are accessible through GEO Series accession number GSE180784 (https://www.ncbi.nlm.nih.gov/geo/query/acc.cgi?acc=GSE180784).

References

Aasen, T., Hodgins, M. B., Edward, M. and Graham, S. V. (2003). The relationship between connexins, gap junctions, tissue architecture and tumour invasion, as studied in a novel in vitro model of HPV-16-associated cervical cancer progression. *Oncogene* **22**, 7969–7980.

Albrengues, J., Bourget, I., Pons, C., Butet, V., Hofman, P., Tartare-Deckert, S., Feral, C. C., Meneguzzi, G. and Gaggioli, C. (2014). LIF Mediates Proinvasive Activation of Stromal Fibroblasts in Cancer. *Cell Reports* **7**, 1664–1678.

Assassi, S., Wu, M., Tan, F. K., Chang, J., Graham, T. A., Furst, D. E., Khanna, D., Charles, J., Ferguson, E. C., Feghali-Bostwick, C., et al. (2013). Skin Gene Expression Correlates of Severity of Interstitial Lung Disease in Systemic Sclerosis. *Arthritis Rheum* **65**, 2917–2927.

Bashir, M., Damineni, S., Mukherjee, G. and Kondaiah, P. (2015). Activin-A signaling promotes epithelial–mesenchymal transition, invasion, and metastatic growth of breast cancer. *npj Breast Cancer* **1**, 1–13.

Basu, S., Totty, N. F., Irwin, M. S., Sudol, M. and Downward, J. (2003). Akt phosphorylates the Yes-associated protein, YAP, to induce interaction with 14-3-3 and attenuation of p73-mediated apoptosis. *Mol Cell* **11**, 11–23.

Brown, R. C. and Davis, T. P. (2002). Calcium modulation of adherens and tight junction function: a potential mechanism for blood-brain barrier disruption after stroke. *Stroke* **33**, 1706–1711.

Brunham, R. C., Binns, B., Guijon, F., Danforth, D., Kosseim, M. L., Rand, F., McDowell, J. and Rayner, E. (1988). Etiology and Outcome of Acute Pelvic Inflammatory Disease. *The Journal of Infectious Diseases* **158**, 510–517.

Caldwell, H. D., Kromhout, J. and Schachter, J. (1981). Purification and partial characterization of the major outer membrane protein of Chlamydia trachomatis. *Infect Immun* **31**, 1161–1176.

Carratelli, C. R., Paolillo, R. and Rizzo, A. (2007). Chlamydia pneumoniae stimulates the proliferation of HUVEC through the induction of VEGF by THP-1. *Int Immunopharmacol* **7**, 287–294.

Cheng, W., Shivshankar, P., Zhong, Y., Chen, D., Li, Z. and Zhong, G. (2008). Intracellular Interleukin-1α Mediates Interleukin-8 Production Induced by Chlamydia trachomatis Infection via a Mechanism Independent of Type I Interleukin-1 Receptor. *Infect. Immun.* **76**, 942–951.

Cheng, D., Jin, L., Chen, Y., Xi, X. and Guo, Y. (2020). YAP promotes epithelial mesenchymal transition by upregulating Slug expression in human colorectal cancer cells. *Int J Clin Exp Pathol* **13**, 701–710.

Chow, J. M., Yonekura, M. L., Richwald, G. A., Greenland, S., Sweet, R. L. and Schachter, J. (1990). The association between Chlamydia trachomatis and ectopic pregnancy. A matched-pair, case-control study. *JAMA* **263**, 3164–3167.

Craig, V. J., Zhang, L., Hagood, J. S. and Owen, C. A. (2015). Matrix metalloproteinases as therapeutic targets for idiopathic pulmonary fibrosis. *Am J Respir Cell Mol Biol* **53**, 585–600.

Dasgupta, I. and McCollum, D. (2019). Control of cellular responses to mechanical cues through YAP/TAZ regulation. *J. Biol. Chem.* **294**, 17693–17706.

Davis, A. P., Grondin, C. J., Johnson, R. J., Sciaky, D., Wiegers, J., Wiegers, T. C. and Mattingly, C. J. (2021). Comparative Toxicogenomics Database (CTD): update 2021. *Nucleic Acids Res* **49**, D1138–D1143.

Davis, A. P., Grondin, C. J., Johnson, R. J., Sciaky, D., McMorran, R., Wiegers, J., Wiegers, T. C. and Mattingly, C. J. The Comparative Toxicogenomics Database: update 2019. *Nucleic Acids Res*.

Dolat, L. and Valdivia, R. H. (2021). An endometrial organoid model of interactions between Chlamydia and epithelial and immune cells. *Journal of Cell Science* **134**, jcs252403.

Dong, J., Feldmann, G., Huang, J., Wu, S., Zhang, N., Comerford, S. A., Gayyed, M. F., Anders, R. A., Maitra, A. and Pan, D. (2007). Elucidation of a universal size-control mechanism in Drosophila and mammals. *Cell* **130**, 1120–1133.

Driscoll, T. P., Cosgrove, B. D., Heo, S.-J., Shurden, Z. E. and Mauck, R. L. (2015). Cytoskeletal to Nuclear Strain Transfer Regulates YAP Signaling in Mesenchymal Stem Cells. *Biophysical Journal* **108**, 2783–2793.

Eckmann, L., Kagnoff, M. F. and Fierer, J. (1993). Epithelial cells secrete the chemokine interleukin-8 in response to bacterial entry. *Infect Immun* **61**, 4569–4574.

Elbediwy, A., Vincent-Mistiaen, Z. I. and Thompson, B. J. (2016). YAP and TAZ in epithelial stem cells: A sensor for cell polarity, mechanical forces and tissue damage. *BioEssays* **38**, 644–653.

Elbediwy, A., Vanyai, H., Diaz-de-la-Loza, M.-C., Frith, D., Snijders, A. P. and Thompson, B. J. (2018). Enigma proteins regulate YAP mechanotransduction. *J Cell Sci* **131**, jcs221788.

Epstein Shochet, G., Brook, E., Bardenstein-Wald, B. and Shitrit, D. (2020). TGF-β pathway activation by idiopathic pulmonary fibrosis (IPF) fibroblast derived soluble factors is mediated by IL-6 trans-signaling. *Respir Res* **21**, 56.

Eto, M., Kirkbride, J. A. and Brautigan, D. L. (2005). Assembly of MYPT1 with protein phosphatase-1 in fibroblasts redirects localization and reorganizes the actin cytoskeleton. *Cell Motil Cytoskeleton* **62**, 100–109.

Fichorova, R. N., Rheinwald, J. G. and Anderson, D. J. (1997). Generation of Papillomavirus-Immortalized Cell Lines from Normal Human Ectocervical, Endocervical, and Vaginal Epithelium that Maintain Expression of Tissue-Specific Differentiation Proteins. *Biol Reprod* **57**, 847–855.

Finch-Edmondson, M. and Sudol, M. (2016). Framework to function: mechanosensitive regulators of gene transcription. *Cell Mol Biol Lett* **21**,.

Fischer, N. (2002). Chlamydia trachomatis infection in cervical intraepithelial neoplasia and invasive carcinoma. *Eur J Gynaecol Oncol* **23**, 247–250.

Futakuchi, A., Inoue, T., Wei, F.-Y., Inoue-Mochita, M., Fujimoto, T., Tomizawa, K. and Tanihara, H. (2018). YAP/TAZ Are Essential for TGF-β2-Mediated Conjunctival Fibrosis. *Invest Ophthalmol Vis Sci* **59**, 3069–3078.

Gali, Y., Ariën, K. K., Praet, M., Van den Bergh, R., Temmerman, M., Delezay, O. and Vanham, G. (2010). Development of an in vitro dual-chamber model of the female genital tract as a screening tool for epithelial toxicity. *Journal of Virological Methods* **165**, 186–197.

Gangwar, I., Sharma, N. K., Panzade, G., Awasthi, S., Agrawal, A. and Shankar, R. (2017). Detecting the Molecular System Signatures of Idiopathic Pulmonary Fibrosis through Integrated Genomic Analysis. *Scientific Reports* **7**, 1554.

Gasparics, Á. and Sebe, A. (2018). MRTFs- master regulators of EMT. *Developmental Dynamics* **247**, 396–404.

Ghosh, S., Ruelke, E. A., Ferrell, J. C., Bodero, M. D., Fields, K. A. and Jewett, T. J. (2020). Fluorescence-Reported Allelic Exchange Mutagenesis-Mediated Gene Deletion Indicates a Requirement for Chlamydia trachomatis Tarp during In Vivo Infectivity and Reveals a Specific Role for the C Terminus during Cellular Invasion. *Infect Immun* **88**, e00841-19.

Grannas, K., Arngården, L., Lönn, P., Mazurkiewicz, M., Blokzijl, A., Zieba, A. and Söderberg, O. (2015). Crosstalk between Hippo and TGFβ: Subcellular Localization of YAP/TAZ/Smad Complexes. *J Mol Biol* **427**, 3407–3415.

Grassie, M. E., Moffat, L. D., Walsh, M. P. and MacDonald, J. A. (2011). The myosin phosphatase targeting protein (MYPT) family: A regulated mechanism for achieving substrate specificity of the catalytic subunit of protein phosphatase type 1δ. *Archives of Biochemistry and Biophysics* **510**, 147–159.

Haggerty, C. L., Gottlieb, S. L., Taylor, B. D., Low, N., Xu, F. and Ness, R. B. (2010). Risk of Sequelae after Chlamydia trachomatis Genital Infection in Women. *The Journal of Infectious Diseases* **201**, S134–S155.

He, C., Mao, D., Hua, G., Lv, X., Chen, X., Angeletti, P. C., Dong, J., Remmenga, S. W., Rodabaugh, K. J., Zhou, J., et al. (2015). The Hippo/YAP pathway interacts with EGFR signaling and HPV oncoproteins to regulate cervical cancer progression. *EMBO Mol Med* **7**, 1426–1449.

Herrera, B., Addante, A. and Sánchez, A. (2017). BMP Signalling at the Crossroad of Liver Fibrosis and Regeneration. *Int J Mol Sci* **19**, 39.

Hu, J. K.-H., Du, W., Shelton, S. J., Oldham, M. C., DiPersio, C. M. and Klein, O. D. (2017). A FAK-YAP-mTOR signaling axis regulates stem cell-based tissue renewal in mice. *Cell Stem Cell* **21**, 91-106.e6.

Huang, Z., Hu, J., Pan, J., Wang, Y., Hu, G., Zhou, J., Mei, L. and Xiong, W.-C. (2016). YAP stabilizes SMAD1 and promotes BMP2-induced neocortical astrocytic differentiation. *Development* **143**, 2398–2409.

Huang, P., Chen, A., He, W., Li, Z., Zhang, G., Liu, Z., Liu, G., Liu, X., He, S., Xiao, G., et al. (2017). BMP-2 induces EMT and breast cancer stemness through Rb and CD44. *Cell Death Discov* **3**, 17039.

Humphrys, M. S., Creasy, T., Sun, Y., Shetty, A. C., Chibucos, M. C., Drabek, E. F., Fraser, C. M., Farooq, U., Sengamalay, N., Ott, S., et al. (2013). Simultaneous Transcriptional Profiling of Bacteria and Their Host Cells. *PLOS ONE* **8**, e80597.

Hung, T.-W., Chu, C.-Y., Yu, C.-L., Lee, C.-C., Hsu, L.-S., Chen, Y.-S., Hsieh, Y.-H. and Tsai, J.-P. (2020). Endothelial Cell-Specific Molecule 1 Promotes Endothelial to Mesenchymal Transition in Renal Fibrosis. *Toxins (Basel)* **12**, 506.

Igietseme, J. U., Omosun, Y., Stuchlik, O., Reed, M. S., Partin, J., He, Q., Joseph, K., Ellerson, D., Bollweg, B., George, Z., et al. (2015). Role of Epithelial-Mesenchyme Transition in Chlamydia Pathogenesis. *PLOS ONE* **10**, e0145198.

Igietseme, J. U., Omosun, Y., Nagy, T., Stuchlik, O., Reed, M. S., He, Q., Partin, J., Joseph, K., Ellerson, D., George, Z., et al. (2018). Molecular Pathogenesis of Chlamydia Disease Complications: Epithelial-Mesenchymal Transition and Fibrosis. *Infection and Immunity* **86**, e00585-17.

Igietseme, J. U., Partin, J., George, Z., Omosun, Y., Goldstein, J., Joseph, K., Ellerson, D., Eko, F. O., Pohl, J., Bandea, C., et al. Epidermal Growth Factor Receptor and Transforming Growth Factor β Signaling Pathways Cooperate To Mediate Chlamydia Pathogenesis. *Infection and Immunity* **88**, e00819-19.

Jeon, Y. K., Kim, C. K., Hwang, K. R., Park, H.-Y., Koh, J., Chung, D. H., Lee, C.-W. and Ha, G.-H. (2017). Pellino-1 promotes lung carcinogenesis via the stabilization of Slug and Snail through K63-mediated polyubiquitination. *Cell Death Differ* **24**, 469–480.

Jewett, T. J., Dooley, C. A., Mead, D. J. and Hackstadt, T. (2008). Chlamydia trachomatis TarP is phosphorylated by src family tyrosine kinases. *Biochem Biophys Res Commun* **371**, 339–344.

Johnson, K. A., Lee, J. K., Chen, A. L., Tan, M. and Sütterlin, C. (2015). Induction and inhibition of CPAF activity during analysis of Chlamydia-infected cells. *Pathog Dis* **73**, 1–8.

Joo, E. E. and Yamada, K. M. (2014). MYPT1 regulates contractility and microtubule acetylation to modulate integrin adhesions and matrix assembly. *Nat Commun* **5**, 3510.

Kendall, R. T. and Feghali-Bostwick, C. A. (2014). Fibroblasts in fibrosis: novel roles and mediators. *Frontiers in Pharmacology* **5**,.

Kim, T., Yang, S.-J., Hwang, D., Song, J., Kim, M., Kyum Kim, S., Kang, K., Ahn, J., Lee, D., Kim, M., et al. (2015). A basal-like breast cancer-specific role for SRF–IL6 in YAP-induced cancer stemness. *Nat Commun* **6**, 10186.

Kiviat, N. B., Wølner-Hanssen, P., Eschenbach, D. A., Wasserheit, J. N., Paavonen, J. A., Bell, T. A., Critchlow, C. W., Stamm, W. E., Moore, D. E. and Holmes, K. K. (1990). Endometrial histopathology in patients with culture-proved upper genital tract infection and laparoscopically diagnosed acute salpingitis. *Am. J. Surg. Pathol.* **14**, 167–175.

Kizu, T., Yoshida, Y., Furuta, K., Ogura, S., Egawa, M., Chatani, N., Hamano, M., Takemura, T., Ezaki, H., Kamada, Y., et al. (2015). Loss of Gab1 adaptor protein in hepatocytes aggravates experimental liver fibrosis in mice. *American Journal of Physiology-Gastrointestinal and Liver Physiology* **308**, G613–G624.

Korol, A., Taiyab, A. and West-Mays, J. A. (2016). Inhibition of MRTF-A/SRF-regulated gene transcription prevents TGFβ-mediated EMT in lens explants. *Invest. Ophthalmol. Vis. Sci.* **57**, 2016–2016.

Korrodi-Gregório, L., Esteves, S. L. C. and Fardilha, M. (2014). Protein phosphatase 1 catalytic isoforms: specificity toward interacting proteins. *Transl Res* **164**, 366–391.

Kyung, S. Y., Kim, D. Y., Yoon, J. Y., Son, E. S., Kim, Y. J., Park, J. W. and Jeong, S. H. (2018). Sulforaphane attenuates pulmonary fibrosis by inhibiting the epithelial-mesenchymal transition. *BMC Pharmacol Toxicol* **19**, 13.

Lachmann, A., Xu, H., Krishnan, J., Berger, S. I., Mazloom, A. R. and Ma'ayan, A. (2010). ChEA: transcription factor regulation inferred from integrating genome-wide ChIP-X experiments. *Bioinformatics* **26**, 2438–2444.

Lachowski, D., Cortes, E., Robinson, B., Rice, A., Rombouts, K. and Del Río Hernández, A. E. (2018). FAK controls the mechanical activation of YAP, a transcriptional regulator required for durotaxis. *FASEB J* **32**, 1099–1107.

Lamouille, S., Xu, J. and Derynck, R. (2014). Molecular mechanisms of epithelial-mesenchymal transition. *Nat Rev Mol Cell Biol* **15**, 178–196.

Lansingh, V. C. (2016). Trachoma. *BMJ Clin Evid* **2016**, 0706.

Lei, Q.-Y., Zhang, H., Zhao, B., Zha, Z.-Y., Bai, F., Pei, X.-H., Zhao, S., Xiong, Y. and Guan, K.-L. (2008). TAZ promotes cell proliferation and epithelial-mesenchymal transition and is inhibited by the hippo pathway. *Mol. Cell. Biol.* **28**, 2426–2436.

Li, N., Feng, Y., Hu, Y., He, C., Xie, C., Ouyang, Y., Artim, S. C., Huang, D., Zhu, Y., Luo, Z., et al. (2018). Helicobacter pylori CagA promotes epithelial mesenchymal transition in gastric carcinogenesis via triggering oncogenic YAP pathway. *J Exp Clin Cancer Res* **37**, 280.

Lutter, E. I., Barger, A. C., Nair, V. and Hackstadt, T. (2013). Chlamydia trachomatis inclusion membrane protein CT228 recruits elements of the myosin phosphatase pathway to regulate release mechanisms. *Cell Rep* **3**, 1921–1931.

Mattingly, C. J., Rosenstein, M. C., Colby, G. T., Forrest, J. N. and Boyer, J. L. (2006). The Comparative Toxicogenomics Database (CTD): a resource for comparative toxicological studies. *J Exp Zool A Comp Exp Biol* **305**, 689–692.

Meinhardt, G., Haider, S., Kunihs, V., Saleh, L., Pollheimer, J., Fiala, C., Hetey, S., Feher, Z., Szilagyi, A., Than, N. G., et al. (2020). Pivotal role of the transcriptional co-activator YAP in trophoblast stemness of the developing human placenta. *Proceedings of the National Academy of Sciences* **117**, 13562–13570.

Miralles, F., Posern, G., Zaromytidou, A.-I. and Treisman, R. (2003). Actin dynamics control SRF activity by regulation of its coactivator MAL. *Cell* **113**, 329–342.

Mital, J. and Hackstadt, T. (2011). Diverse Requirements for Src-Family Tyrosine Kinases Distinguish Chlamydial Species. *mBio*.

Mo, J.-S., Yu, F.-X., Gong, R., Brown, J. H. and Guan, K.-L. (2012). Regulation of the Hippo–YAP pathway by protease-activated receptors (PARs). *Genes Dev* **26**, 2138–2143.

Mori, M., Triboulet, R., Mohseni, M., Schlegelmilch, K., Shrestha, K., Camargo, F. D. and Gregory, R. I. (2014). Hippo signaling regulates microprocessor and links cell-density-dependent miRNA biogenesis to cancer. *Cell* **156**, 893–906.

Morita, T., Mayanagi, T. and Sobue, K. (2007). Dual roles of myocardin-related transcription factors in epithelial–mesenchymal transition via slug induction and actin remodeling. *J Cell Biol* **179**, 1027–1042.

Ness, R. B., Soper, D. E., Richter, H. E., Randall, H., Peipert, J. F., Nelson, D. B., Schubeck, D., McNeeley, S. G., Trout, W., Bass, D. C., et al. (2008). Chlamydia Antibodies, Chlamydia Heat Shock Protein, and Adverse Sequelae After Pelvic Inflammatory Disease: The PID Evaluation and Clinical Health (PEACH) Study. *Sexually Transmitted Diseases* **35**, 129–135.

Ng, B., Dong, J., D'Agostino, G., Viswanathan, S., Widjaja, A. A., Lim, W.-W., Ko, N. S. J., Tan, J., Chothani, S. P., Huang, B., et al. (2019). Interleukin-11 is a therapeutic target in idiopathic pulmonary fibrosis. *Sci Transl Med* **11**, eaaw1237.

Ng, B., Cook, S. A. and Schafer, S. (2020). Interleukin-11 signaling underlies fibrosis, parenchymal dysfunction, and chronic inflammation of the airway. *Exp Mol Med* **52**, 1871–1878.

Noguchi, S., Saito, A. and Nagase, T. (2018). YAP/TAZ Signaling as a Molecular Link between Fibrosis and Cancer. *Int J Mol Sci* **19**,.

Nogueira, A. T., Braun, K. M. and Carabeo, R. A. (2017). Characterization of the Growth of Chlamydia trachomatis in In Vitro-Generated Stratified Epithelium. *Front Cell Infect Microbiol* **7**, 438.

O'Keefe, E. J., Briggaman, R. A. and Herman, B. (1987). Calcium-induced assembly of adherens junctions in keratinocytes. *J Cell Biol* **105**, 807–817.

Panciera, T., Azzolin, L., Cordenonsi, M. and Piccolo, S. (2017). Mechanobiology of YAP and TAZ in physiology and disease. *Nat Rev Mol Cell Biol* **18**, 758–770.

Paolillo, R., Iovene, M. R., Carratelli, C. R. and Rizzo, A. (2012). Induction of VEGF and MMP-9 Expression by Toll-like Receptor 2/4 in Human Endothelial Cells Infected with Chlamydia Pneumoniae. *Int J Immunopathol Pharmacol* **25**, 377–386.

Papiris, S. A., Tomos, I. P., Karakatsani, A., Spathis, A., Korbila, I., Analitis, A., Kolilekas, L., Kagouridis, K., Loukides, S., Karakitsos, P., et al. (2018). High levels of IL-6 and IL-8 characterize early-on idiopathic pulmonary fibrosis acute exacerbations. *Cytokine* **102**, 168–172.

Park, J., Kim, D.-H., Shah, S. R., Kim, H.-N., Kshitiz, Kim, P., Quiñones-Hinojosa, A. and Levchenko, A. (2019). Switch-like enhancement of epithelial-mesenchymal transition by YAP through feedback regulation of WT1 and Rho-family GTPases. *Nat Commun* **10**, 2797.

Patel, A. L., Chen, X., Wood, S. T., Stuart, E. S., Arcaro, K. F., Molina, D. P., Petrovic, S., Furdui, C. M. and Tsang, A. W. (2014). Activation of epidermal growth factor receptor is required for Chlamydia trachomatis development. *BMC Microbiology* **14**, 277.

Pedrosa, A. T., Murphy, K. N., Nogueira, A. T., Brinkworth, A. J., Thwaites, T. R., Aaron, J., Chew, T.-L. and Carabeo, R. A. (2020). A post-invasion role for Chlamydia type III effector TarP in modulating the dynamics and organization of host cell focal adhesions. *J Biol Chem* **295**, 14763–14779.

Phan, T. H. G., Paliogiannis, P., Nasrallah, G. K., Giordo, R., Eid, A. H., Fois, A. G., Zinellu, A., Mangoni, A. A. and Pintus, G. (2021). Emerging cellular and molecular determinants of idiopathic pulmonary fibrosis. *Cell Mol Life Sci* **78**, 2031–2057.

Piccolo, S., Dupont, S. and Cordenonsi, M. (2014). The biology of YAP/TAZ: hippo signaling and beyond. *Physiol Rev* **94**, 1287–1312.

Piersma, B., Bank, R. A. and Boersema, M. (2015). Signaling in Fibrosis: TGF-β, WNT, and YAP/TAZ Converge. *Front Med (Lausanne)* **2**, 59.

Pocaterra, A., Romani, P. and Dupont, S. (2020). YAP/TAZ functions and their regulation at a glance. *Journal of Cell Science* **133**,.

Porcella, S. F., Carlson, J. H., Sturdevant, D. E., Sturdevant, G. L., Kanakabandi, K., Virtaneva, K., Wilder, H., Whitmire, W. M., Song, L. and Caldwell, H. D. (2015). Transcriptional Profiling of Human Epithelial Cells Infected with Plasmid-Bearing and Plasmid-Deficient Chlamydia trachomatis. *Infect. Immun.* **83**, 534–543.

Price, M. J., Ades, A. E., Soldan, K., Welton, N. J., Macleod, J., Simms, I., DeAngelis, D., Turner, K. M. and Horner, P. J. (2016). *Pelvic inflammatory disease and tubal factor infertility*. NIHR Journals Library.

Rajić, J., Inic-Kanada, A., Stein, E., Dinić, S., Schuerer, N., Uskoković, A., Ghasemian, E., Mihailović, M., Vidaković, M., Grdović, N., et al. (2017). Chlamydia trachomatis Infection Is Associated with E-Cadherin Promoter Methylation, Downregulation of E-Cadherin Expression,

and Increased Expression of Fibronectin and α-SMA-Implications for Epithelial-Mesenchymal Transition. *Front Cell Infect Microbiol* **7**, 253.

Rasmussen, S. J., Eckmann, L., Quayle, A. J., Shen, L., Zhang, Y. X., Anderson, D. J., Fierer, J., Stephens, R. S. and Kagnoff, M. F. (1997). Secretion of proinflammatory cytokines by epithelial cells in response to Chlamydia infection suggests a central role for epithelial cells in chlamydial pathogenesis. *J Clin Invest* **99**, 77–87.

Robertson, J. N., Ward, M. E., Conway, D. and Caul, E. O. (1987). Chlamydial and gonococcal antibodies in sera of infertile women with tubal obstruction. *J Clin Pathol* **40**, 377–383.

Salton, F., Volpe, M. C. and Confalonieri, M. (2019). Epithelial¯Mesenchymal Transition in the Pathogenesis of Idiopathic Pulmonary Fibrosis. *Medicina (Kaunas)* **55**, E83.

Scidmore, M. A. and Hackstadt, T. (2001). Mammalian 14-3-3beta associates with the Chlamydia trachomatis inclusion membrane via its interaction with IncG. *Mol Microbiol* **39**, 1638–1650.

Sero, J. E. and Bakal, C. (2017). Multiparametric Analysis of Cell Shape Demonstrates that β-PIX Directly Couples YAP Activation to Extracellular Matrix Adhesion. *Cell Syst* **4**, 84-96.e6.

Shehat, M. G., Aranjuez, G. F., Kim, J. and Jewett, T. J. (2021). The Chlamydia trachomatis Tarp effector targets the Hippo pathway. *Biochem Biophys Res Commun* **562**, 133–138.

Smoot, R. L., Werneburg, N. W., Sugihara, T., Hernandez, M. C., Yang, L., Mehner, C., Graham, R. P., Bronk, S. F., Truty, M. J. and Gores, G. J. (2018). Platelet-derived growth factor regulates YAP transcriptional activity via Src family kinase dependent tyrosine phosphorylation. *Journal of Cellular Biochemistry* **119**, 824–836.

Song, X., Chen, H.-X., Wang, X.-Y., Deng, X.-Y., Xi, Y.-X., He, Q., Peng, T.-L., Chen, J., Chen, W., Wong, B. C.-Y., et al. (2013). H. pylori-encoded CagA disrupts tight junctions and induces invasiveness of AGS gastric carcinoma cells via Cdx2-dependent targeting of Claudin-2. *Cell Immunol* **286**, 22–30.

Stephens, R. S. (2003). The cellular paradigm of chlamydial pathogenesis. *Trends in Microbiology* **11**, 44–51.

Strickland, S., Brimer, N., Lyons, C. and Vande Pol, S. B. (2018). Human Papillomavirus E6 interaction with cellular PDZ domain proteins modulates YAP nuclear localization. *Virology* **516**, 127–138.

Sugihara, T., Werneburg, N. W., Hernandez, M. C., Yang, L., Kabashima, A., Hirsova, P., Yohanathan, L., Sosa, C., Truty, M. J., Vasmatzis, G., et al. (2018). YAP Tyrosine Phosphorylation and Nuclear Localization in Cholangiocarcinoma Cells Are Regulated by LCK and Independent of LATS Activity. *Mol Cancer Res* **16**, 1556–1567.

Szeto, S. G., Narimatsu, M., Lu, M., He, X., Sidiqi, A. M., Tolosa, M. F., Chan, L., Freitas, K. D., Bialik, J. F., Majumder, S., et al. (2016). YAP/TAZ Are Mechanoregulators of TGF-β-Smad Signaling and Renal Fibrogenesis. *JASN* ASN.2015050499.

Taylor, H. R., Burton, M. J., Haddad, D., West, S. and Wright, H. (2014). Trachoma. *The Lancet* **384**, 2142–2152.

Vite, A., Zhang, C., Yi, R., Emms, S. and Radice, G. L. (2018). α-Catenin-dependent cytoskeletal tension controls Yap activity in the heart. *Development* **145**, dev149823.

Wei, H., Wang, F., Wang, Y., Li, T., Xiu, P., Zhong, J., Sun, X. and Li, J. (2017). Verteporfin suppresses cell survival, angiogenesis and vasculogenic mimicry of pancreatic ductal adenocarcinoma via disrupting the YAP-TEAD complex. *Cancer Sci* **108**, 478–487.

Weström, L., Joesoef, R., Reynolds, G., Hagdu, A. and Thompson, S. E. (1992). Pelvic inflammatory disease and fertility. A cohort study of 1,844 women with laparoscopically verified disease and 657 control women with normal laparoscopic results. *Sex Transm Dis* **19**, 185–192.

Widjaja, A. A., Singh, B. K., Adami, E., Viswanathan, S., Dong, J., D'Agostino, G. A., Ng, B., Lim, W. W., Tan, J., Paleja, B. S., et al. (2019). Inhibiting Interleukin 11 Signaling Reduces Hepatocyte Death and Liver Fibrosis, Inflammation, and Steatosis in Mouse Models of Nonalcoholic Steatohepatitis. *Gastroenterology* **157**, 777-792.e14.

Wynn, T. (2008). Cellular and molecular mechanisms of fibrosis. *J Pathol* **214**, 199–210.

Xiang, D.-M., Sun, W., Ning, B.-F., Zhou, T.-F., Li, X.-F., Zhong, W., Cheng, Z., Xia, M.-Y., Wang, X., Deng, X., et al. (2018). The HLF/IL-6/STAT3 feedforward circuit drives hepatic stellate cell activation to promote liver fibrosis. *Gut* **67**, 1704–1715.

Xu, J., Lamouille, S. and Derynck, R. (2009). TGF-beta-induced epithelial to mesenchymal transition. *Cell Res* **19**, 156–172.

Yamaguchi, H. and Taouk, G. M. (2020). A Potential Role of YAP/TAZ in the Interplay Between Metastasis and Metabolic Alterations. *Frontiers in Oncology* **10**,.

Yang, Y., Lara, A., Rutebemberwa, A. and Schmidt, E. (2017). Heparanase contributes to idiopathic pulmonary fibrosis via regulation of A20/TNFAIP3 expression. *The FASEB Journal* **31**, 656.14-656.14.

Yin, X., Yi, H., Wang, L., Wu, W., Wu, X., Yu, L., Yin, X., Yi, H., Wang, L., Wu, W., et al. (2016). RSPOs facilitated HSC activation and promoted hepatic fibrogenesis. *Oncotarget* **7**, 63767–63778.

Yu, G., Wang, L.-G., Han, Y. and He, Q.-Y. (2012). clusterProfiler: an R Package for Comparing Biological Themes Among Gene Clusters. *OMICS: A Journal of Integrative Biology* **16**, 284–287.

Zadora, P. K., Chumduri, C., Imami, K., Berger, H., Mi, Y., Selbach, M., Meyer, T. F. and Gurumurthy, R. K. (2019). Integrated Phosphoproteome and Transcriptome Analysis Reveals Chlamydia-Induced Epithelial-to-Mesenchymal Transition in Host Cells. *Cell Rep* **26**, 1286-1302.e8.

Zagurovskaya, M., Shareef, M. M., Das, A., Reeves, A., Gupta, S., Sudol, M., Bedford, M. T., Prichard, J., Mohiuddin, M. and Ahmed, M. M. (2009). EGR-1 forms a complex with YAP-1 and upregulates Bax expression in irradiated prostate carcinoma cells. *Oncogene* **28**, 1121–1131.

Zanconato, F., Forcato, M., Battilana, G., Azzolin, L., Quaranta, E., Bodega, B., Rosato, A., Bicciato, S., Cordenonsi, M. and Piccolo, S. (2015). Genome-wide association between YAP/TAZ/TEAD and AP-1 at enhancers drives oncogenic growth. *Nat Cell Biol* **17**, 1218–1227.

Zeng, G., Xun, W., Wei, K., Yang, Y. and Shen, H. (2016). MicroRNA-27a-3p regulates epithelial to mesenchymal transition via targeting YAP1 in oral squamous cell carcinoma cells. *Oncology Reports* **36**, 1475–1482.

Zhao, X.-H., Laschinger, C., Arora, P., Szászi, K., Kapus, A. and McCulloch, C. A. (2007a). Force activates smooth muscle alpha-actin promoter activity through the Rho signaling pathway. *J. Cell. Sci.* **120**, 1801–1809.

Zhao, B., Wei, X., Li, W., Udan, R. S., Yang, Q., Kim, J., Xie, J., Ikenoue, T., Yu, J., Li, L., et al. (2007b). Inactivation of YAP oncoprotein by the Hippo pathway is involved in cell contact inhibition and tissue growth control. *Genes Dev.* **21**, 2747–2761.

Zhao, B., Ye, X., Yu, J., Li, L., Li, W., Li, S., Yu, J., Lin, J. D., Wang, C.-Y., Chinnaiyan, A. M., et al. (2008). TEAD mediates YAP-dependent gene induction and growth control. *Genes Dev* **22**, 1962–1971.

Figures and Tables

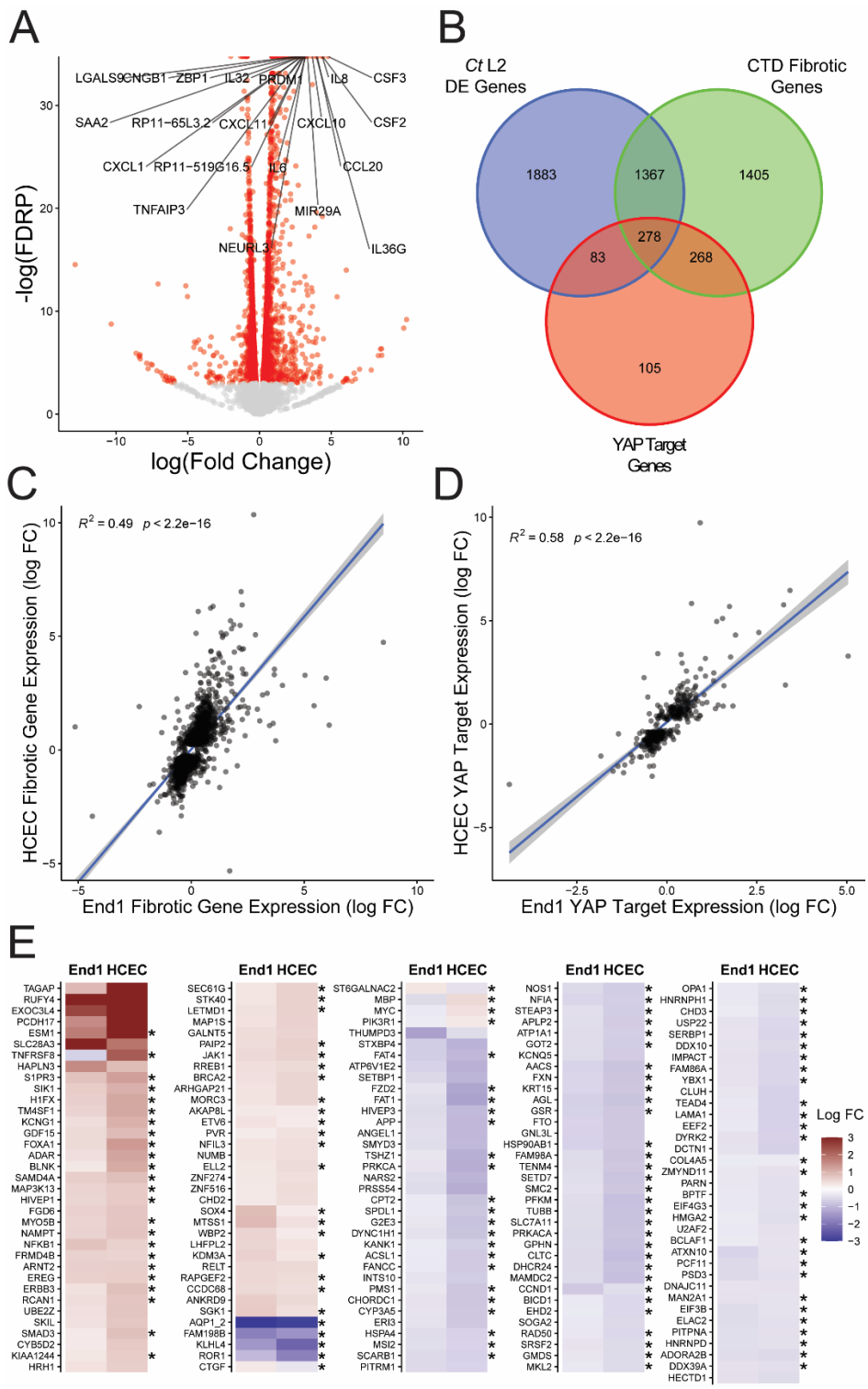

Figure 1. *Chlamydia* infection induces a fibrosis-associated host transcriptomic response consistent with YAP activation.
(A) Volcano plot of genes identified via bulk RNA-sequencing of End1/E6E7 immortalized epithelial cells during infection with *Chlamydia trachomatis* (*Ct*) serovar L2, at 24 hours post-infection (hpi). n = 3, with a minimum of $3x10^7$ unstranded single reads per replicate with a mean length of 150 bp. All fold changes are relative to the mock-infected control; red dots: false discovery rate p-value (FDRP) ≤ 0.05.
(B) Venn diagram of differentially expressed genes identified in (A) cross-referenced with the Comparative Toxicogenomics Database (CTD) of pro-fibrotic genes, as well as the ChIP Enrichment Analysis (ChEA) database of YAP target genes. See also Supplemental Figure S1, and Supplemental Datasets S1 and S2.
(C) Scatter plot of gene expression of pro-fibrotic (CTD), differentially expressed genes in *Ct* serovar L2-infected End1/E6E7 cells (End1s, x-axis) and primary human cervical epithelial cells (HCECs, y-axis). All fold changes are relative to each cell type's respective mock-infected control; blue line: linear regression model of correlation; grey shading: 95% confidence interval. R^2 and p-values calculated using Pearson's correlation.
(D) Scatter plot of gene expression of YAP-responsive (ChEA), differentially expressed genes in *Ct* serovar L2-infected End1s (x-axis) and HCECs (y-axis). All fold changes are relative to each cell type's respective mock-infected control; blue line: linear regression model of correlation; grey shading: 95% confidence interval. R^2 and p-values calculated using Pearson's correlation.
(E) Heatmap of YAP target gene expression in *Ct* serovar L2-infected End1s (left columns) and HCECs (right columns). All fold changes are relative to each cell type's respective mock-infected control; only genes differentially expressed (FDRP ≤ 0.05) in both cell types are shown. Asterisks: members of the Comparative Toxicogenomics Database (CTD) of pro-fibrotic genes.

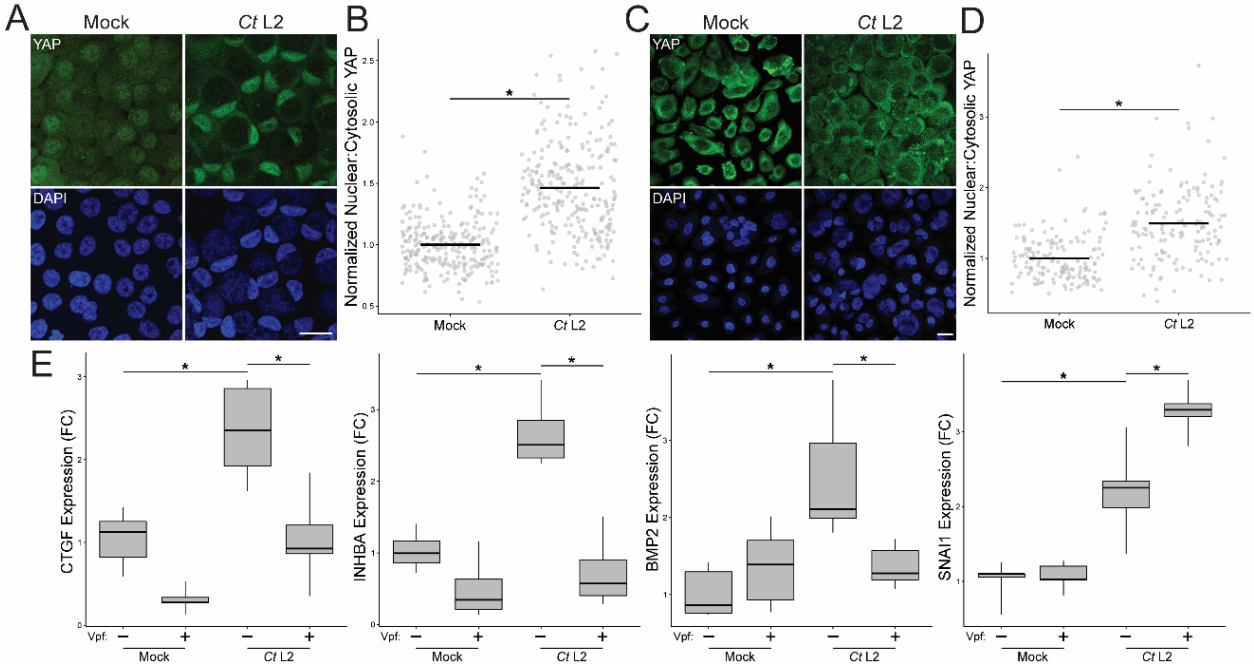

Figure 2. *Chlamydia* infection induces host YAP nuclear translocation and YAP/TEAD-dependent gene expression.
(A) Representative micrographs of YAP (green) translocation into the nuclei (blue) of confluent mock- and *Ct* L2-infected End1 cells at 24 hpi. Scale bar: 20 μm.
(B) Quantification of YAP nuclear translocation in (A) as a ratio of nuclear to cytosolic YAP fluorescence. n = 5 biological replicates, 50 cells measured per sample. Black bars: group means; asterisks: p-values ≤ 0.05, using pairwise Wilcoxon rank sum tests and Bonferroni's correction for multiple comparisons.
(C) Representative micrographs of YAP (green) translocation into the nuclei (blue) of confluent mock- and *Ct* L2-infected primary human cervical epithelial cells at 24 hpi. Scale bar: 20 μm.
(D) Quantification of YAP nuclear translocation in (C) as a ratio of nuclear to cytosolic YAP fluorescence. n = 5 biological replicates, 50 cells measured per sample. Black bars: group means; asterisks: p-values ≤ 0.05, using pairwise Wilcoxon rank sum tests and Bonferroni's correction for multiple comparisons.
(E) Expression of CTGF, INHBA, BMP2, and SNAIL at 24 hpi in mock- and *Ct* L2-infected End1 cells treated with the YAP-TEAD inhibitor verteporfin (Vpf, 5 μM for 16 h starting at 8 hpi), as measured by quantitative RT-PCR. n = 6 biological replicates; fold changes are relative to mean expression of the mock-infected and untreated control. Asterisks: p-values ≤ 0.05, using pairwise Student's t-tests and Bonferroni's correction for multiple comparisons.

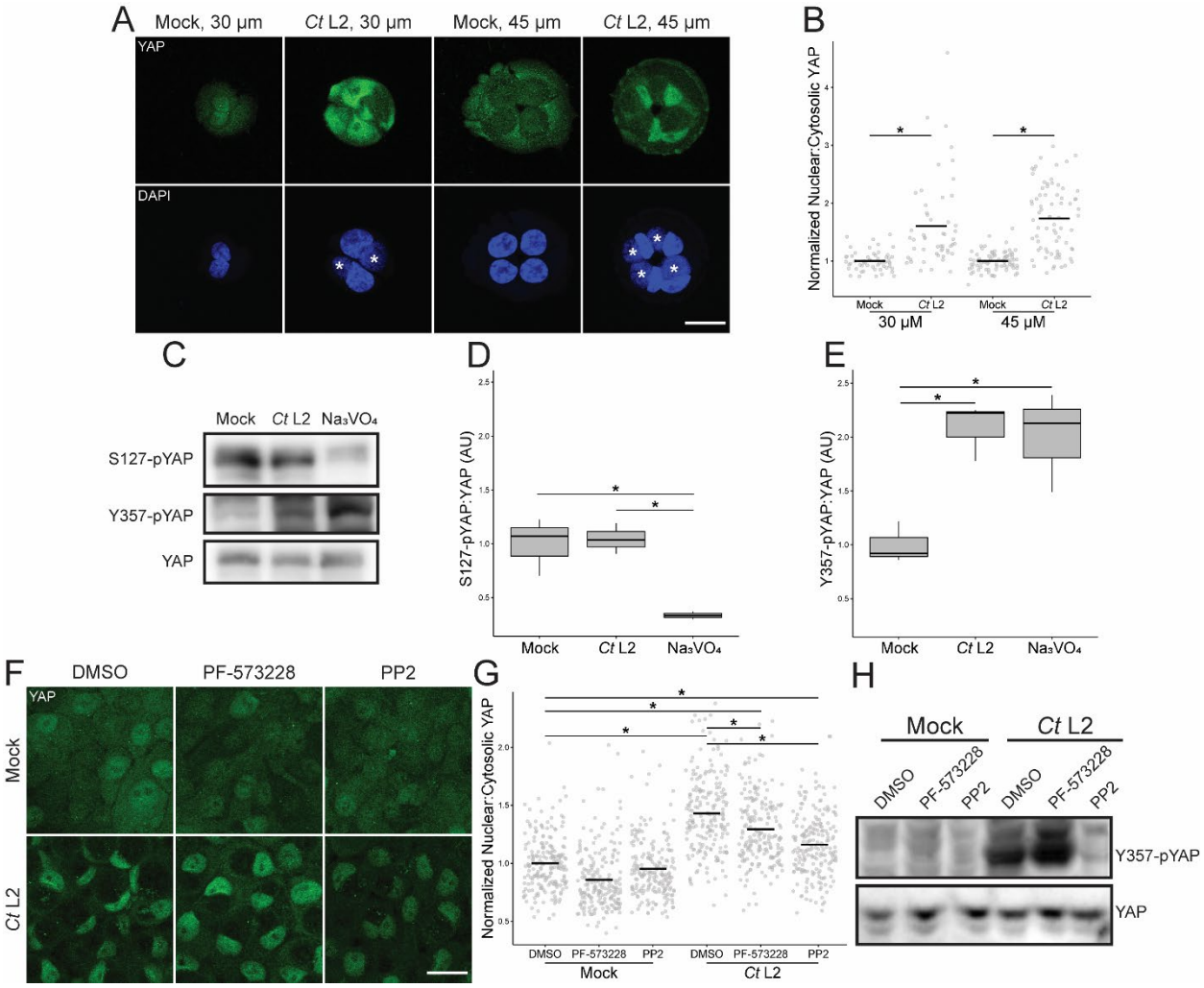

Figure 3. *Chlamydia* infection activates host YAP independent of Hippo-mediated YAP inhibition.
(A) Representative micrographs of YAP (green) translocation into the nuclei (blue) at 24 hpi of mock- and *Ct* L2-infected End1 cells cultured in small cell clusters using 30 µm (1-2 cells) and 45 µm (2-4 cells) micropatterns. Asterisks: chlamydial inclusions; scale bar: 20 µm.
(B) Quantification of YAP nuclear translocation in (D) as a ratio of nuclear to cytosolic YAP fluorescence. n = 3 biological replicates, with a minimum of 5 fields measured per sample. Black bars: group means; asterisks: p-values ≤ 0.05, using pairwise Wilcoxon rank sum tests and Bonferroni's correction for multiple comparisons.
(C) Representative Western blot of YAP phosphorylation of mock- and *Ct* L2-infected or sodium orthovanadate-treated (Na_3VO_4, 10 mM for 1 h at 23 hpi) End1 cells at 24 hpi.
(D, E) Densitometric quantification of YAP phosphorylation at S127 (D) and Y357 (E), normalized to total YAP. n = 3 biological replicates; asterisks: p-values ≤ 0.05, using pairwise Student's t-tests and Bonferroni's correction for multiple comparisons.
(F) Representative micrographs of YAP translocation at 24 hpi in confluent mock- and *Ct* L2-infected End1 cells treated with the FAK inhibitor PF-573228 (5 µM for 24 h), Src inhibitor PP2 (10 µM for 24 h), or DMSO. Scale bar: 20 µm.
(G) Quantification of YAP nuclear translocation in (F). n = 4 biological replicates, 50 cells measured per

sample. Black bars: group means; asterisks: p-values ≤ 0.05, using pairwise Wilcoxon rank sum tests and Bonferroni's correction for multiple comparisons. See also Supplemental Figure S2.
(H) Representative Western blot of YAP tyrosine phosphorylation of mock- and *Ct* L2-infected End1 cells at 24 hpi, treated with the FAK inhibitor PF-573228 (5 μM for 24 h), Src inhibitor PP2 (10 μM for 24 h), or DMSO.

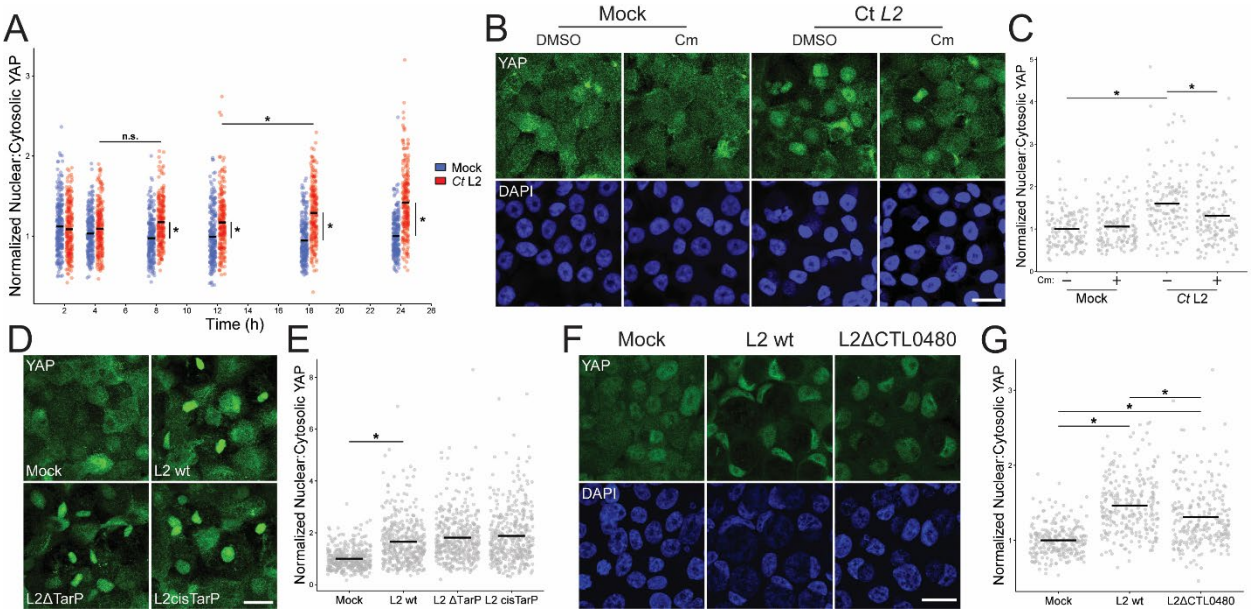

Figure 4. Chlamydial YAP activation requires the myosin-modulating effector CTL0480.
(A) Quantification of YAP nuclear translocation at 2, 4, 8, 12, 18, and 24 hpi in confluent mock- and *Ct* L2-infected End1 cells as a ratio of nuclear to cytosolic YAP fluorescence. n = 5 biological replicates, 50 cells measured per sample. Blue dots: mock-infected cells, red dots: *Ct* L2-infected cells, black bars: group means, asterisks: p-value ≤ 0.05, using pairwise Wilcoxon rank-sum tests and Bonferroni's correction for multiple comparisons.
(B) Representative micrographs of YAP (green) translocation at 18 hpi in confluent mock- and *Ct* L2-infected End1 cells treated with chloramphenicol (Cm, 50 µg/mL for 1 h at 17 hpi) or DMSO. Scale bar: 20 µm.
(C) Quantification of YAP nuclear translocation in (B). n = 3 biological replicates, 50 cells measured per sample. Black bars: group means; asterisks: p-values ≤ 0.05, using pairwise Wilcoxon rank-sum tests and Bonferroni's correction for multiple comparisons.
(D) Representative micrographs of YAP translocation at 24 hpi in confluent End1s either mock-infected or infected with wild-type *Ct* L2, a L2ΔTarP mutant strain, or the cis-complemented strain (L2cisTarP). Scale bars: 20 µm.
(E) Quantification of YAP nuclear translocation in (D). n = 6 biological replicates, 50 cells measured per sample. Black bars: group means; asterisks: p-values ≤ 0.05, using pairwise Wilcoxon rank-sum tests and Bonferroni's correction for multiple comparisons.
(F) Representative micrographs of YAP translocation at 24 hpi in confluent End1s either mock-infected or infected with wild-type Ct L2 or a L2ΔCTL0480 mutant strain. Scale bars: 20 µm.
(G) Quantification of YAP nuclear translocation in (F). n = 5 biological replicates, 50 cells measured per sample. Black bars: group means; asterisks: p-values ≤ 0.05, using pairwise Wilcoxon rank-sum tests and Bonferroni's correction for multiple comparisons. See also Supplemental Figure S2.

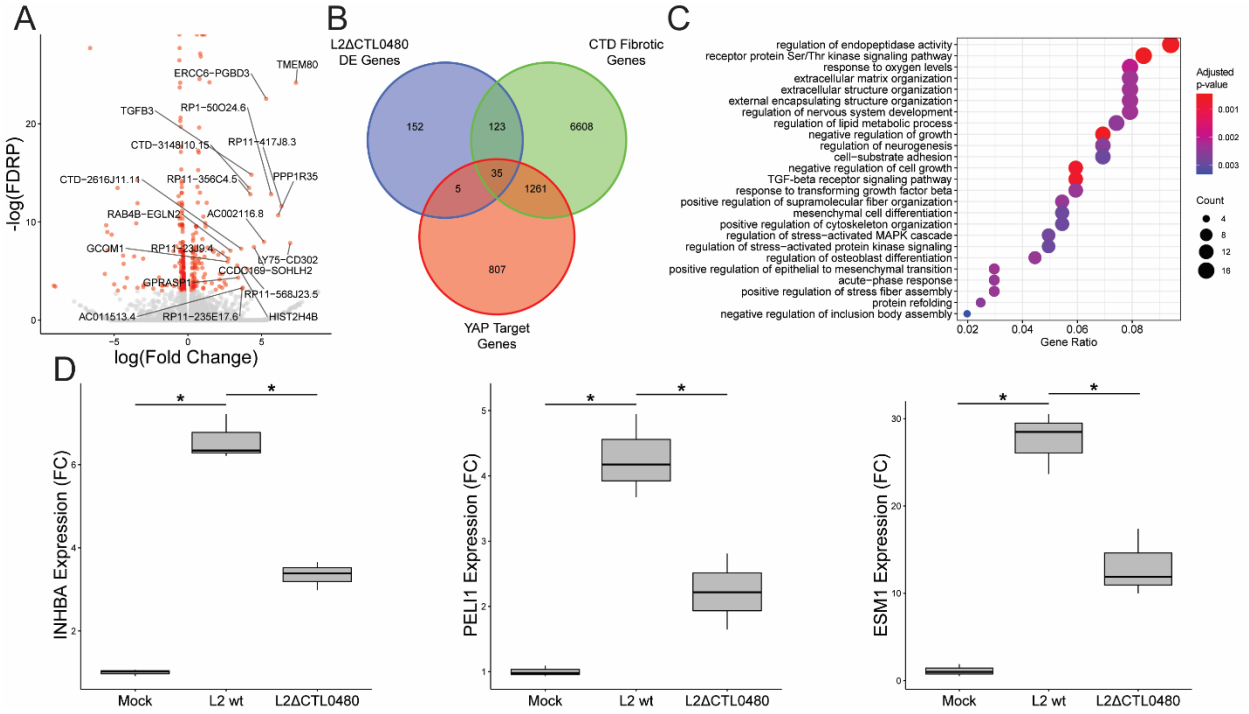

Figure 5. Loss of CTL0480 attenuates *Chlamydia*-induced pro-fibrotic gene expression.
(A) Volcano plot of genes identified via bulk RNA-sequencing of End1 cells during infection with *Ct* L2 *wild-type* or L2ΔCTL0480, at 24 hours post-infection (hpi). n = 3 biological replicates, with a minimum of $4x10^7$ unstranded single reads per replicate with a mean length of 150 bp. All fold changes are relative to the wild-type infection; red dots: false discovery rate p-value (FDRP) ≤ 0.05.
(B) Venn diagram of differentially expressed genes identified in (a), cross-referenced with the Comparative Toxicogenomics Database (CTD) of pro-fibrotic genes, as well as the ChIP Enrichment Analysis (ChEA) database of YAP target genes.
(C) Dot plot of top 25 significantly enriched GO terms identified in the L2ΔCTL0480-deficient infection. Color: adjusted p-value, size: number of GO term-associated genes differentially expressed (FDRP ≤ 0.05) relative to the wild-type infection. See also Supplemental Dataset S3 and Supplemental Figure S4.
(D) Expression of SNAIL, INHBA, and PELI1 at 24 hpi in mock-, wild-type *Ct* L2-, and *Ct* L2ΔCTL0480-infected End1 cells, as measured by quantitative RT-PCR. n = 3 biological replicates; fold changes are relative to mean expression of the mock-infected and untreated control. Asterisks: p-values ≤ 0.05, using pairwise Student's t-tests and Bonferroni's correction for multiple comparisons.

Transcription Factor	Induced Targets	Repressed Targets	Mean Fold Change
IRF1	55	0	2.60
STAT1	34	9	1.44
STAT3	255	80	2.46
SMAD2	126	31	9.11
SMAD3	162	57	4.89
TEAD4	67	29	1.21
EGR1	292	101	2.11
YAP1	81	36	1.24
MYCN	61	56	-62.65
MYBL1	2	4	-0.49
CRX	21	18	-2.02

Table 1: Cross-referencing of RNA-sequencing results with ChEA transcription factor target database reveals induction of pro-EMT transcription factor targets.

Gene	Fold Change	FDRP	Associated Pathology
RSPO3	14.95	9.56E-04	Hepatic fibrosis (Yin et al., 2016)
TNFAIP3	7.97	0.00E+00	Idiopathic pulmonary fibrosis (Yang et al., 2017)
AFF3	4.79	1.30E-02	Idiopathic pulmonary fibrosis (Gangwar et al., 2017)
GBP2	3.00	1.36E-02	Hepatic fibrosis (Kizu et al., 2015)
MMP9	3.13	4.59E-07	Idiopathic pulmonary fibrosis (Craig et al., 2015)
HAPLN3	2.96	1.86E-02	Interstitial lung disease (Assassi et al., 2013)
LIF	2.55	0.00E+00	Fibroblast motility, ECM modification (Albrengues et al., 2014)
BMP2	2.41	4.83E-02	Hepatic fibrosis (Herrera et al., 2017)

Table 2: YAP target genes induced by *Ct* infection are associated with fibrotic pathology.

Supplemental Information

Supplemental Dataset S1. Summary of differentially expressed genes detected in bulk RNA-sequencing of mock- and *Ct* serovar L2-infected End1/E6E7 immortalized epithelial cells (End1s). All fold-changes expressed relative to mock-infected control. See enclosed file: “Supplemental Dataset S1.xlsx”.

Supplemental Dataset S2. “Summary of the cross-referencing of Table S1A data with the ChIP Enrichment Analysis (ChEA) database of transcription factor target genes. See enclosed file: Supplemental Dataset S2.xlsx”.

Supplemental Dataset S3. Summary of differentially expressed genes detected in bulk RNA-sequencing of mock- and *Ct* serovar L2-infected primary human cervical epithelial cells (HCECs). All fold-changes expressed relative to mock-infected control. See enclosed file: “Supplemental Dataset S3.xlsx”.

Supplemental Dataset S4. Summary of differentially expressed genes detected in bulk RNA-sequencing of wild-type L2- and L2ΔCTL0480-infected End1s. All fold changes expressed relative to wild-type infected control. See enclosed file: “Supplemental Dataset S4.xlsx”.

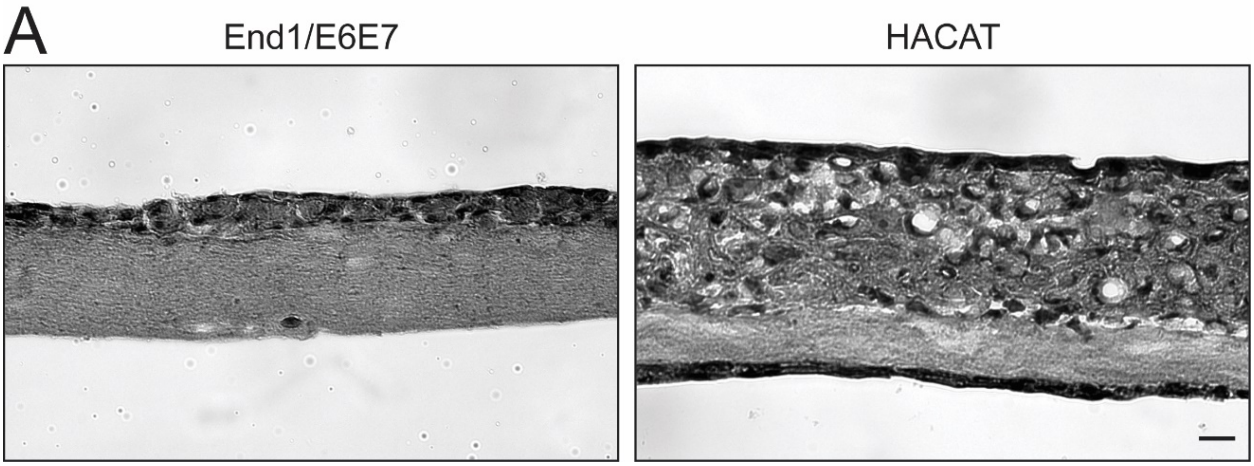

Supplemental Figure S1. End1 E6/E7-immortalized epithelial cells in organotypic culture do not exhibit morphology consistent with malignant HPV-associated transformation.
(A) Greyscale, bright-field micrograph of hematoxylin/eosin-stained 20 µm sections of End1 (left) and HaCaT (right) RAFT cultures. Scale bar: 20 µm.

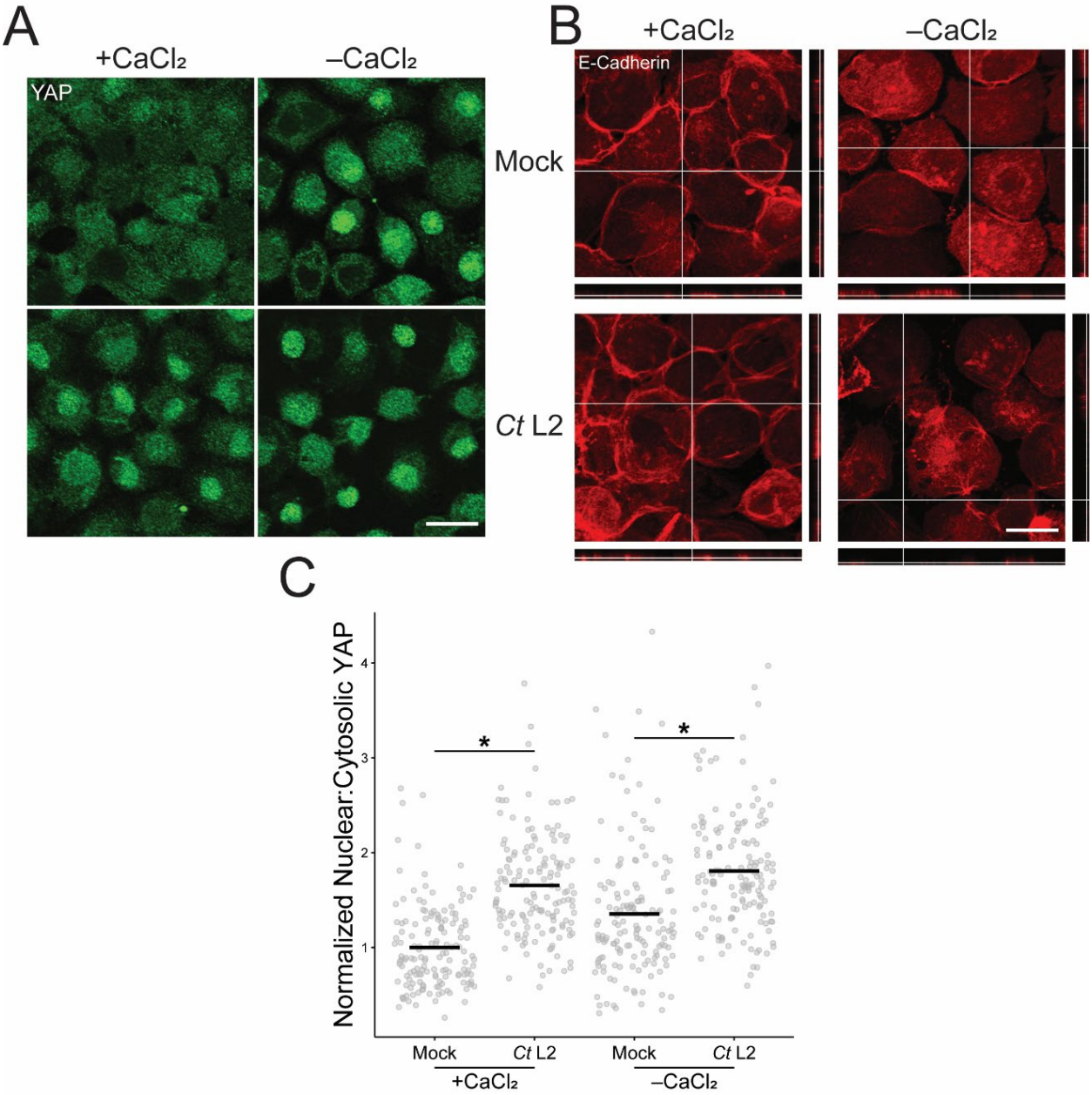

Supplemental Figure S2. *Chlamydia* infection enhances YAP nuclear translocation in the Hippo-attenuated condition of adherens junction disruption.
(A) Representative micrographs of YAP (green) translocation at 24 hpi in confluent mock- and *Ct* L2-infected End1 cells cultured in calcium-replete (+$CaCl_2$, 0.4 mM) or calcium-deplete (-$CaCl_2$) keratinocyte serum-free media. Scale bar: 20 µm.
(B) Representative micrographs of E-cadherin (red) localization at 24 hpi in confluent mock- and Ct L2-infected End1 cells cultured in calcium-replete (+$CaCl_2$, 0.4 mM) or calcium-deplete (-CaCl2) keratinocyte serum-free media. Right sidebar: ZY-plane orthogonal view; left sidebar: XZ-plane orthogonal view; scale bar: 20 µm.

(C) Quantification of YAP nuclear translocation in (A). n = 3 biological replicates, 50 cells measured per sample. Black bars: group means; asterisks: p-values ≤ 0.05, using pairwise Wilcoxon rank sum tests and Bonferroni's correction for multiple comparisons.

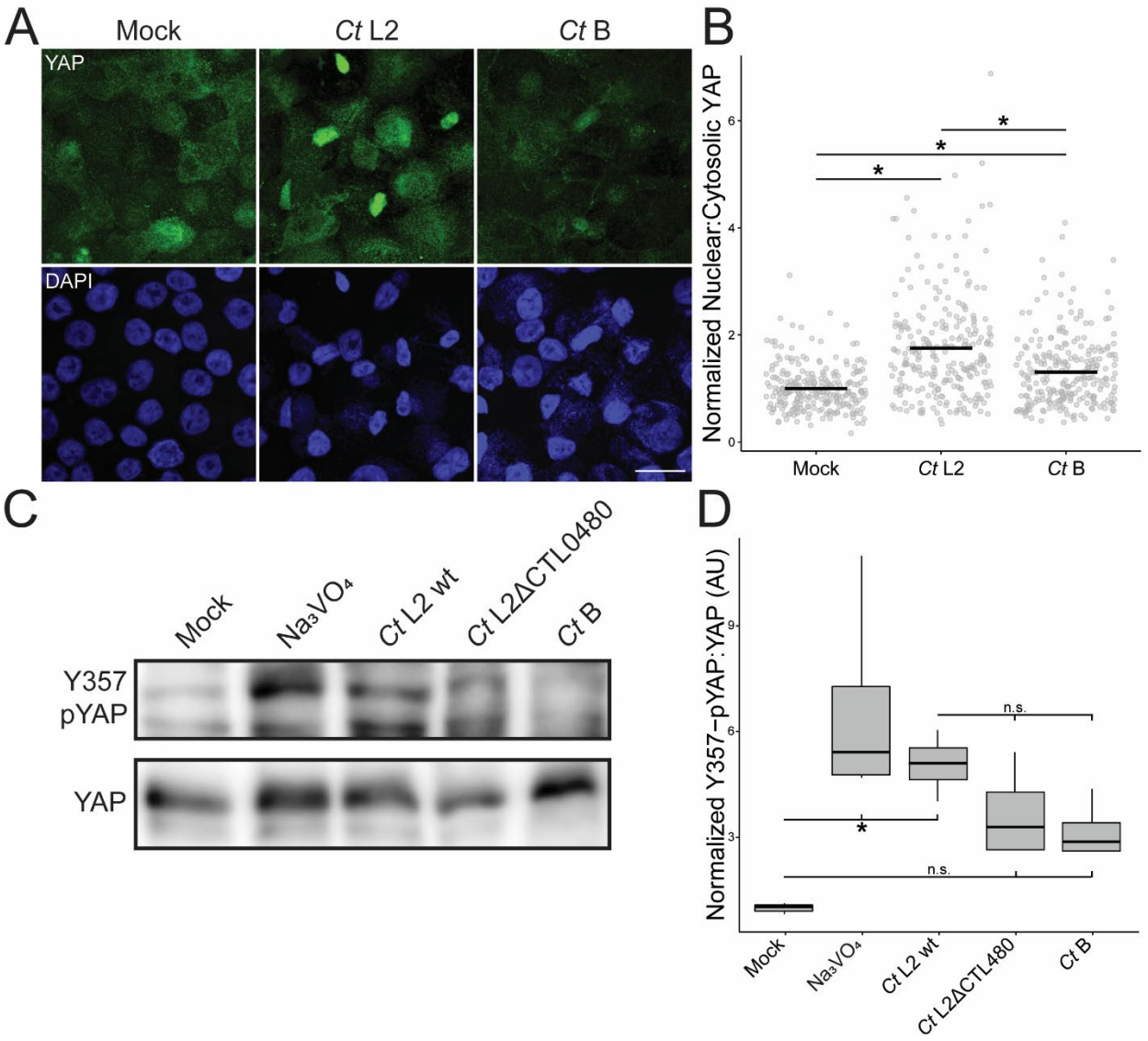

Supplemental Figure S3. The CTL0480-deficient *Ct* serovar B exhibits an attenuated YAP nuclear translocation phenotype.
(A) Representative micrographs of YAP (green) translocation at 24 hpi in confluent mock-, *Ct* L2-, or *Ct* B-infected End1 cells. Scale bar: 20 µm.
(B) Quantification of YAP nuclear translocation in (A). n = 5 biological replicates, 50 cells measured per sample. Black bars: group means; asterisks: p-values ≤ 0.05, using pairwise Wilcoxon rank sum tests and Bonferroni's correction for multiple comparisons.
(C) Representative Western blot of YAP Y357 phosphorylation of mock-,*Ct* L2-, *Ct* L2ΔCTL0480-, or Ct B-infected or sodium orthovanadate-treated (Na_3VO_4, 10 mM for 1 h at 23 hpi) End1 cells at 24 hpi.

(D) Densitometric quantification of YAP Y357 phosphorylation, normalized to total YAP. n = 4 biological replicates; asterisks: p-values ≤ 0.05, using pairwise Student's t-tests and Bonferroni's correction for multiple comparisons.

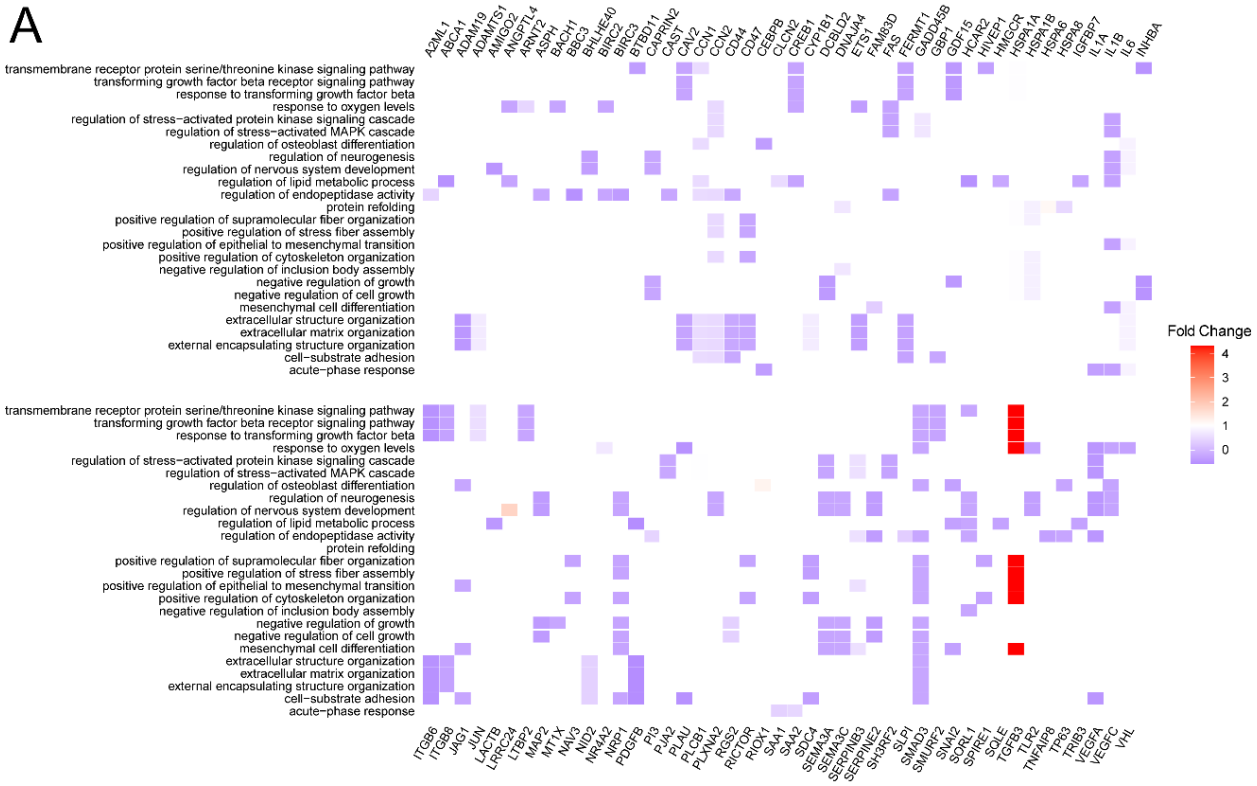

Supplemental Figure S4. L2ΔCTL0480-infected End1 cells exhibit attenuated expression of EMT-associated genes.
(A) Heat map of enriched GO term gene expression. Color: fold change relative to the wild-type infection. Only the top 25 significantly enriched GO terms are shown. See also Supplemental Dataset S4.